

Literature Review

Laser beam machining (LBM) has proven its applications and advantages over almost all the range of engineering materials. It offers its competences from macro machining to micro and nano-machining of simple-to-complex shapes. The flipside of LBM is the existence of universal problems associated with its thermal ablation mechanism. In order to alleviate or reduce the inherent problems of LBM, a massive research has been done during the past decade and in turn build a relatively new route of laser-hybrid processes. The hybrid approaches in laser ablation have demonstrated much improved results in terms of material removal rate, surface integrity, geometrical tolerances, thermal damage, metallurgical alterations and many more.

1 Background

Conventional machining (CM) is no doubt greatly applicable for wide variety of materials. However, shaping of hard to machine materials alongside the complex geometries impose some limitations. Difficult to machine materials such as titanium and nickel alloys, superalloys, ceramics and metal matrix composites are not easy to deal with CM processes. Similarly, complex machining characteristics (3-D milling, high aspect drilling, taper free holes, crack free edges etc.) and fragile jobs (ultrathin sheets, wafers etc.) call for some competitive process. In connection, modern components and products like spinning nozzles, turbine blades and fuel injectors require high standard of machining results.

There are two common practices to accept such challenges. One is to employ non-conventional machining (NCM) process and the other is assisting the CM process with some non-conventional machining (NCM) technique. Laser beam machining (LBM) is much promising in this regard especially dealing with almost whole range of engineering materials [53]. Although the process is slow but it offers

great advantages over the conventional machining processes like non-contact and non-wearing tool, independence of material hardness, good surface finish and precise cut quality. Laser beam cutting is superior to any cutting method conventional or non-conventional because of material versatility, no wear or change of tool, high material utilization, production flexibility, high accuracy and edge quality.

Instead of direct material removal, however, the laser energy is also used for heating [54], melting [55] or assisting the other machining processes. In these scenarios the process is termed as laser assisting machining (LAM) [56]. It is more widely used to enrich the CM potentials especially for hard-to-machine materials. The literature is clustered with laser assisted conventional turning which majorly contribute to reduce the cutting forces, improve the tool life and process throughput. In the last decade, the trend is switching from traditional LBM to hybrid LBM by coupling some other phenomenon/process to LBM setup. The coupling process could be chemical etching [57, 58], electrochemical machining [59], ultrasonic machining [60, 61], electric discharge machining [62], water jet [63] and liquid film [64] etc. The common motive to this hybrid approach is to minimize/alleviate the traditional LBM's drawbacks such as thermal damage, heat affected zone (HAZ), low ablation rate, cracking and melt re-deposition.

In this chapter, the competitive advantages of LBM, LAM and fluidly immersed hybrid laser machining are reviewed. The emphasis is kept to generate a bit clear understanding of material removal mechanisms in each regime and the impact of machining parameters on part features. In the end, new challenges and future directions are proposed.

2 Laser Beam Machining (LBM)

Laser beam machining (LBM) is a material removal process governed by focusing a coherent beam of monochromatic light of laser on the substrate surface. The beam is generated and focused by fiber optics and/or combination of reflecting mirrors and delivered to the target through beam delivery system. The process is energized by mishmash of different energies such as thermal, mechanical, chemical and thermo-mechanical. Material is rapidly removed in the form of tiny particles.

2.1 Physical Factors Affecting the Process

The material removal in the laser milling is mainly a function of laser characteristics and the material properties. This dual role becomes more complex when laser beam interacts with the material. This interaction is affected by many process as well as material parameters.

2.1.1 Laser Radiation Features

Laser (Light Amplification by Stimulated Emission of Radiation) is a high-energy beam of electromagnetic radiations. The light, photon, moves as a wave through space, but behaves as a particle of energy when it bumps into matter [65]. Laser radiations can be controlled and modulated by an ordered train of pulses with known pulse duration and pulse frequency. The accumulation of these pulses generates energy which is released for ultra-short time period and results, what we require, extremely high power. Moreover, when laser beam is focused to a small spot size (100 μm or less) it significantly increase the energy density (fluence) and the power density (intensity) around the spotted zone. This extremely high intensity (10^{13} – 10^{18} W/cm^2) is sufficient to cause the melting of material which cannot be possible by conventional processes [66].

2.1.2 Substrate Material Features

The material response against laser radiation varies based upon many factors. Ablation occurs only when material absorbs enough energy to get melted or vaporized. So the incident wavelength must be matched with the material to be worked. Higher the absorption the efficient could be the milling results. Thermal conductivity is another prime key which decides the energy dissipation from laser interaction zone to the bulk material. Less is the thermal conductivity better is the expected material removal. The ablation also depends upon the associated material transition energies primarily including latent heat of vaporization and latent heat of melting.

2.2 *Laser Ablation Mechanism*

The laser ablation depends on optical properties of laser beam, laser system's configuration, working parameters, plasma shield, sample position with respect to focal plane and mechanical, optical and thermal properties of substrate material. When laser radiations strike on the substrate surface, electrons in the substrate gets on excited by the laser photons. This absorbs the photon energy and generates significant heat which is transferred to the close premises of the material in picosecond interval resulting in high temperature. The temperature reaches so high that it leads the material to melting or vaporization state. The light absorption phenomenon is classically presented by Beer-Lambert Law [67]. It states that when a light of certain wavelength is transmitted through the material, its absorption depends on the material path length and is totally independent of the incident intensity. When the materials reaches to a certain electron density, it absorbs photon energy sufficient enough to initiate the ablation. This critical energy is termed as laser fluence threshold [66]. Laser intensity can be enhanced either by reducing the

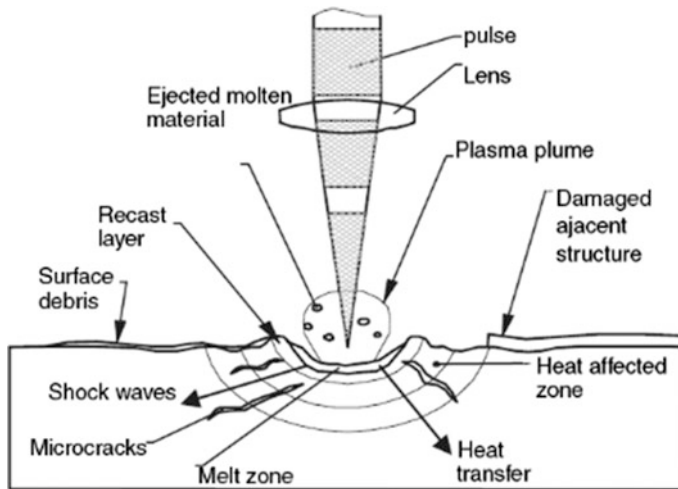


Fig. 1 Nanosecond and longer pulse laser ablation [66]

focal spot or by increasing the laser power [68]. After the substrate reaching at melting point the melt liquid phase appears in the form of thin layer at the localized interaction zone. The temperature of the melt liquid phase rapidly rises by the subsequent incoming pulses to reach the melt phase at evaporation state (plasma state). This yields a high pressure which is very commonly termed as recoil pressure. The recoil pressure squeezes the liquid up from the interaction zone and ejects the material out (Fig. 1) [66]. The rapid rise of temperature further amplifies the magnitude of recoil pressure in a range of hundreds of MPa. Yilbas et al. [69] reported this pressure to 1 GPa for mild steel and stainless steel. The recoil pressure exerts impact loading on the substrate surface that generate elastic-plastic wave in the surface. This is more commonly known as shock wave propagation [70]. The shock wave locally dislocates the surface grains at the shock-affected region. Due to such dislocations and impact loading of shock wave enrich the target material's surface hardness. The ejection of melt debris is another main concern of LBM which is generally derived by some assisting gas (shielding gas). Irrespective to this, the recoil pressure is considered as main material ejecting agent [71].

2.3 Laser Beam Milling

The application of laser beam milling is equally suited for metals and non-metals. Among the metals titanium alloy (Ti6Al4V) and nickel based superalloys (particularly Inconel 718) are mainly treated under laser. It is worth noting that the laser beam milling of nickel based superalloys is highly uncommon while cutting of nickel alloys can be very widely seen. However, laser beam milling is also widely

employed on non-metals especially structural ceramics, glass, polymers and carbon fiber reinforced polymers (CFRP). Material removal rate, thermal damage, heat affected zone, taper and delamination influenced/caused by laser parameters is widely evaluated by many researchers. Numerical, mathematical and thermal models are the tools to predict their values and distributions in advance to experimental plan. Though, these estimations are well established for non-metals as compared to metals.

2.3.1 Ablation Mechanism of Laser Beam Milling

The general mechanism of laser ablation is described in the previous section. The material removal mechanism for milling is almost the same. However, it could somewhat differ by processing conditions and machined features. That difference is correspondingly included wherever it is encountered. Therefore, it is not felt necessary to include here the details.

2.3.2 Laser Beam Milling of Titanium Alloys

Alpha case (an oxygen enriched alloy layer) is commonly formed in forged titanium alloys during the manufacturing process and it reduces the service life of the material. This layer is normally removed mechanically or chemically. Laser beam milling with short pulse width can remove the alpha case layer and allow to reach the titanium alloy layer extremely smoother (R_a —110 nm) without any surface cracks [72]. Laser pulse can also be employed in different modes particularly in two; single pulse and multi-pulse. These modes generate varying level of fluences. The interaction of these modes at higher pulse count and varying fluences with titanium alloys show surface character in terms of craters, melt pools at periphery, cracks and TiO_2 layer [73]. The ablation rate under these modes varies for different materials. To explain this variation, in a study of [74] the researchers employed single shot laser pulses of 10 picosecond having 1064 nm wavelength and fluence range of 2–25 J/cm² on aluminum, Ti6Al4V and gold. The mechanism behind this variation was reported as the electron heat capacity and electron-phonon coupling time. Aluminum and titanium take shortest coupling time of 4 and 7 ps while gold takes over 100 ps. In general, it is inferred that ablation depth per pulse increases with increase in laser fluence. Steel and copper also exhibits similar behavior under these pulse and fluence ranges [75]. Biomedical implants made of Ti6Al4V if treated under high laser fluence (140 J/Cm²) of Nd:YAG laser can generate higher wettability characteristics than mechanically roughened surface. In this treated way the cell attachment becomes high and wide spread than any other condition and the implant shows no sign of infection [76]. Femtosecond laser treatments allow to achieve various surface textures on such biomedical implants. These textures consist of nanoscale laser-induced periodic surface structures (LIPSS), nano-pillars, micro porous columns and complex textures which are now a days being adopted

for implants due to different wettability characteristics [77]. The increase in fluence also alter the microstructure and wear resistance of implant positively in terms of surface grain size and hardness [78]. Laser re-melting (LR) is another alternative to elongate the grain size without affecting the corrosion and wear resistance properties. There is no phase transformation in LR. That's why corrosion resistance remains unchanged. Though, as a consequent of microstructural changes the micro-hardness increases with increase in fluence. At high fluences (10 and 30 kJ/cm²) two zones appear in titanium alloy named as melt zone (MZ) and heat affected zone (HAZ) but at low to medium fluences (0.5 and 10 kJ/cm²), there exist three zones named as melt zone (MZ), heat affected zone (HAZ) and base metal (BM) [79].

2.3.3 Laser Beam Milling of Nickel Alloys

Inconel 718 is considered as hard-to-machine material due to difficulties of machining as a results of its extremely tough nature. Laser ablation is a competent process allowing to machine nickel alloys irrespective to their hardness. Nd:YAG, CO₂ and femtosecond lasers are generally employed to deal with nickel alloys machining. During laser cutting the influence of laser parameters on cut quality has remained the researchers' core interest. Some of the research is dedicated towards the temperature measurements along the cut edges, circumferential and longitudinal (depth wise) directions. Heat transfer and its contribution towards microstructural alteration is also somewhat found in the literature. In general, laser beam cutting is widely attempted to cut the nickel based superalloys. For the production of 3D geometrical features in nickel based superalloys the LBM is very rarely employed as per available open literature. For example, Ahmed et al. [80] fabricated 3D micro-channels in Inconel 718 by Nd:YAG laser. The effect of laser parameters on geometrical and microstructural aspects are evaluated. The micro-channel's depth and width is mainly driven by laser scanning speed.

The part quality produced by laser cutting highly depends on surface finish of cut section. In order to achieve high quality cut section the excessive dross attachment and micro-cracks should be avoided. The surface roughness decreases with the increase in cutting speed. The optimal cutting speed ranges 8–10 cm/s for 1–2 mm thick sheet. For the Inconel 718 having thickness of 2 mm and cut by Nd:YAG laser requires even low cutting speeds for the same results. However, the surface roughness of cut section does not significantly depends on laser power for <2 mm thick sheets [81]. Laser cutting of mild steel with identical thickness and CW Nd:YAG laser parameters also yields the same inferences [82]. In addition, the oxidation reaction takes place in the kerf width forming some oxide layers. As the composition of Inconel 718 contains more reactive constituents such as chromium, nickel and niobium than the mild steel. Therefore, the heat energy caused by the oxidation reaction produces deeper grooves with higher peaks and valleys in the cut section of Inconel 718. The average surface roughness ($R_a \sim 3 \mu\text{m}$) can be achieved by increasing the laser power to 4 kW and assist gas pressure of 19 bar.

The increase in laser power and cutting speed however increase the taper ratio of top and bottom cut edges. But increase in assist gas pressure shrinks the top edge taper. There is a relationship, developed by [83], between laser parameters and kerf width depicting that the minimum kerf width of the cut section lies in the range of 0.53–0.61 mm. Recast layer thickness becomes high for high laser power but can positively be controlled by increasing the assist gas pressure and the cutting speed up to 3 cm/s. One of the common feature of laser cutting is the formation of striations on cut sections. These striations are classified into two regions. To certain penetration depth there exists a smooth and finer striation structure. The striations are straight and parallel in this region. At the second region it becomes zigzag to the bottom of cut. This variation is explained by the divergence behavior of the laser beam along the workpiece thickness. As the beam diverges through the material thickness it becomes less intense compare to top of cut. The striation frequency is almost independent of power but can be controlled by cutting speed adjustments. The heights of the first region decreases while the second region heights increase by increase in cutting speed irrespective to laser power [84].

2.3.4 Laser Beam Milling of Ceramics and CFRP

Carbon fibers (CF) need approximately 98% of energy absorption for its ablation [85]. For sublimating a single CF layer (10 μm thickness) under the area of 50 μm radius, more than 10 mJ of absorbed energy is required [68]. If the absorbs energy is too much then melting will occur and if it is too little then insufficient thermal stresses would be resulted [86]. On the other hand edge remains unaffected with respect to crack, delamination and thermal damaging [87]. Quality of the CFRP strongly depends on operating wavelength as well. The HAZ gets doubled for 1064 nm wavelength as compared to 532 and 355 nm [85]. The “perpendicular heat flow model” is helpful to achieve the minimum thermal damage in matrix materials and to understand the damage mechanism [68]. In addition to other laser oriented parameters, temperature dependent absorptivity and thermo-physical properties (conduction, convection and radiation based heat transfer) of the material also plays important role in quality of laser beam milling in ceramics [88]. These parameters mainly affect the MRR and side tapering during 3-D machining of ceramics [89].

2.3.5 Parametric Effects in Laser Beam Milling

Pulsed wave as well as continuous wave (CW) Nd:YAG and CO₂ lasers are commonly experienced in laser beam milling. Ytterbium fiber and excimer laser are also getting popular in the last decade. Generally, the average power of 8–20 W with relatively high pulse frequency (10–80 kHz) is suitable for laser beam milling of metals and non-metals. High laser power (~ 500 W) is also adopted by some

Table 1 Parametric window of LBM

Process	Work material	Investigations	Laser type	Laser Parameters				Modeling	References
				Avg./peak power	Wavelength	Pulse width	Frequency	Spot/beam dia.	
Laser beam milling	Metals	<ul style="list-style-type: none"> • Titanium alloys • Nickel alloys • Mild steel • Stainless steel 	<ul style="list-style-type: none"> • CW CO₂ • Nd:YVO₄ • Nd:YAG • Ytterbium fiber 	550 W 10 W 2–8 W 30 W	532 nm 1064 nm	10 µs	10 kHz 20–80 kHz 30–50 kHz	5 mm 40 µm 70 µm 30 µm	[71, 80, 92, 99–101, 124]
	Non-Metals	<ul style="list-style-type: none"> • Alumina • SiC • Si₃N₄ • Magnesia • Al/Al₂O₃-MMC • CFRP • Glass • ABS • PMMA 	<ul style="list-style-type: none"> • Pulsed Nd:YAG • CW Nd:YAG • CW CO₂ • Ytterbium fiber 	470 W 10–23 W 20 W	1.06 µm 355 µm 532 µm 1064 nm	0.5 ms 10 ps	20 Hz 600–680 Hz 200 kHz	0.5 mm 10 µm 3 mm 32 µm 73 µm	[68, 85–89, 102, 123]
Laser beam drilling/ trepanning	Metals	<ul style="list-style-type: none"> • Thermal distribution • Recast layer • HAZ • hole taper • MRR • Spatter • Cracking 	<ul style="list-style-type: none"> • CO₂ laser • Nd:YVO₄ • Pulsed Nd:YAG 	2 kW 18 W 14 kW 400 W 10 kW 75 W	532 nm 1.06 µm	10 ns 5 ms 10 ms 120 ns	20 kHz 20 Hz 1 kHz 10 Hz	0.5 mm 300 µm 100 µm	[71, 104–106, 109, 115, 119, 125]
	Non-Metals	<ul style="list-style-type: none"> • MRR • Hole taper • Hole circularity 	<ul style="list-style-type: none"> • Pulsed Nd:YAG • Ps laser 		1064 nm	0.5 ms 60 ps	20 Hz 250 kHz	35 µm	[102, 103, 112, 114]

researchers but not in common. The only parametric difference (metals v/s no-metals) is in pulse frequency (up to 600 kHz) and spot diameter (up to 10 μm) for non-metals. For reference, first half of the Table 1 shows the detailed parametric window for laser milling. There is lack of information in the studies about the proper reasoning of these parametric variations.

The major problems of laser beam milling are low MRR, recast layer, delamination, cracking, thermal damage and HAZ. Residual stresses, white layer and work hardening layers, as well as microstructural alterations are reported by Ulutan and Ozel [90] as the potential problems associated with laser ablation particularly on titanium and nickel alloys. Although the problems are mostly same for metals and non-metals but their controlling and dependence is different for different materials. For example, certain metallic alloys have high viscosity in molten state due to which it is difficult to ensure clean cut. There are number of limitations of laser machining of metals and the influence of operating parameters on productivity as well as on the quality of the machined surface. Productivity depends mainly on the frequency of the laser pulse. Aluminum alloy (AA 6056) behaves differently at higher frequencies ($f \geq 5500$ Hz) than stainless steel (X3CrNi18-10) and titanium alloy (Ti6Al4V). The surface roughness of the machined surface depends mainly on pulse frequency and, secondarily, on sweep speed. Cicală et al. [91] obtained the lowest levels of roughness ($R_a \approx 2$ μm) with the highest frequencies ($f \geq 7500$ Hz) and with low sweep speeds (6 mm/s). Pulsed laser micro-polishing can be employed to reduce the surface roughness and mill scratches. High pulse frequency (4 kHz) is the key parameter to control. However, surface cracking occurs when polishing is done in air but it can be avoided by using shielding gas. Argon gas shielding demonstrates good results. It validates a crack free surface and a reduction in average surface roughness by a factor of two for Ti6Al4V [92].

2.3.6 Temperatures and Stress Field Distribution

Laser heating in the presence of assisting gas usually employed to evaluate the temperature and stress field distributions. It is also used to evaluate the microstructural alterations due to laser irradiations. During laser heating high power (in kW) laser is generally used with relatively larger (in millimeters) spot diameters. The heat dissipates/penetrates along the three axis (x, y and z) at the same time but the distribution pattern varies for each direction. Along the x direction (the laser movement direction) the heating cycle is more temporal and uniform than cooling cycle. As the heat generated beneath the spot distributes along x-axis at one region and in the meantime the laser beam moves in the same direction at new region. In this way the new region starts heating from some preliminary value (say half of region 1's heat) and further heated to peak value by laser beam. This results in peaks and valleys in heating cycle (Fig. 2). The valleys are in fact average surface temperature along the x direction. However during cooling cycle the temperature gradient reduces sharply due to laser spot movement. Temperature variations along y-axis usually follows the Gaussian distribution (as of laser beam) during both the

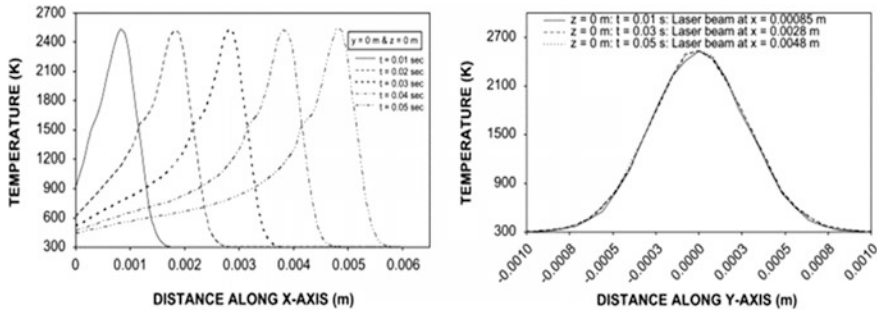


Fig. 2 Temperature distribution along the x-axis and y-axis at different heating periods [93]

cycles. But it could be somewhat different if the laser beam follows other distributions. Along the z-axis the temperature at the surface remains maximum and decays gradually in the surface vicinity and the decay becomes sharp in the area next to the surface vicinity. Laser heating by high power, CO₂ laser allows to achieve crack free surface of Inconel 718 and depth of laser treated region extends almost 50 μm below the surface. Laser heating improves the micro-hardness at the surface due to the grain refinement and high cooling rates provided by assist gas [93]. High pressure nitrogen gas is most common in assisting gases.

The measurements of surface temperature is always considered as the tedious task. It is usually very difficult or often impossible to directly measure surface temperatures introduced by machining processes such as deep drilling. Reissig et al. [94] presented a post-mortem-method, which allows to determine maximum temperatures during machining by measuring the local vanadium concentration in transformed β -grains in Ti6Al4V. The pseudo-temperature can be detected in volumes as small as 50 nm³ and can even be obtained directly at free surfaces [94]. In order to investigate the complicated transient thermal phenomena in laser micromachining, it is essential to accurately measure time-resolved temperatures of workpiece resulted from the transient laser-material interaction. While numerous analytic and numerical models have also been developed, little experimental results are available for a solid understanding of transient thermal phenomena in nanosecond pulsed laser micromachining. Choi and Li [95] demonstrated that the micro thin film thermocouples (TFTCs) can be useful in measuring the transient temperatures at micrometers away from the laser-material interaction region on the workpiece during laser micromachining, and the measured data could be utilized to validate and improve existing analytical and numerical models.

2.3.7 Laser Induced Periodic Structures

Use of high average power density or laser fluence (0.28–30 J/cm²) and low number of over-scans cause the material to become porous with high surface

roughness. As the average power density increases, microscopic holes (pores) with average dimensions of 300–400 nm appear on the surface. However, by increasing the over-scans (5–90) with low fluences the pores can be avoided with low surface roughness. But, for very low average power densities the surface morphology of irradiated areas comprises of ripples. The appearance of such ripples is a general phenomenon of laser ablation termed as laser induced periodic surface structures (LIPSS) [96]. This phenomenon has been detected in many different materials from metals and semiconductors. According to [97] formation of ripples is a result of an interference between the incident laser beam and surface electromagnetic wave randomly dispersed on the surface asperities. However, stated by [98], the material surface also undergoes some self-organization processes during its relaxation from a state of high non-equilibrium following the ultrafast heating by femtosecond laser. It could also be possible that the formation of ripples is the result of such processes.

2.3.8 Laser Beam Milling with Auxiliary Concepts

To challenge the traditional problems of dry laser ablation, laser beam milling is also interestingly connected with some auxiliary concepts such as combining grit blasting with laser milling. It can eject the molten material more efficiently. Under same operating conditions as for traditional laser beam milling, this dual process allows to achieve 100% MRR and 15% and 60% reduction in HAZ and surface roughness respectively for mild steel, stainless steel and titanium alloys [99]. Similarly, MRR and quality of laser beam milling can be enriched by laser-induced plasma micro-machining (LIPMM) process. When the laser beam is focused, on the workpiece submerged in the dielectric, deionization of the dielectric occurs resulting in plasma spot formation. It is claimed that the process can machine, more competitively, a variety of materials including metals, ceramics and polymers [100]. Recast layer is considered as major drawback of laser beam milling. Instead of elimination and avoidance of melt recasting, the utilization of recast layer can be experienced in a positive sense. Lee et al. [101] adopted this technique of piling up the recast layer to synthesize the micro pins (see Fig. 3). Using combination of recast layers and their successive piling-up can generate micro pin array of length 603 μm in steel.

2.4 Laser Beam Drilling/Trepanning

Laser trepanning and drilling is another member of the LBM family. It allows to drill and trepan macro as well as micro holes in non-metals as well as in metals and alloys. Laser beam drilling in different ceramics can be seen in Fig. 4.

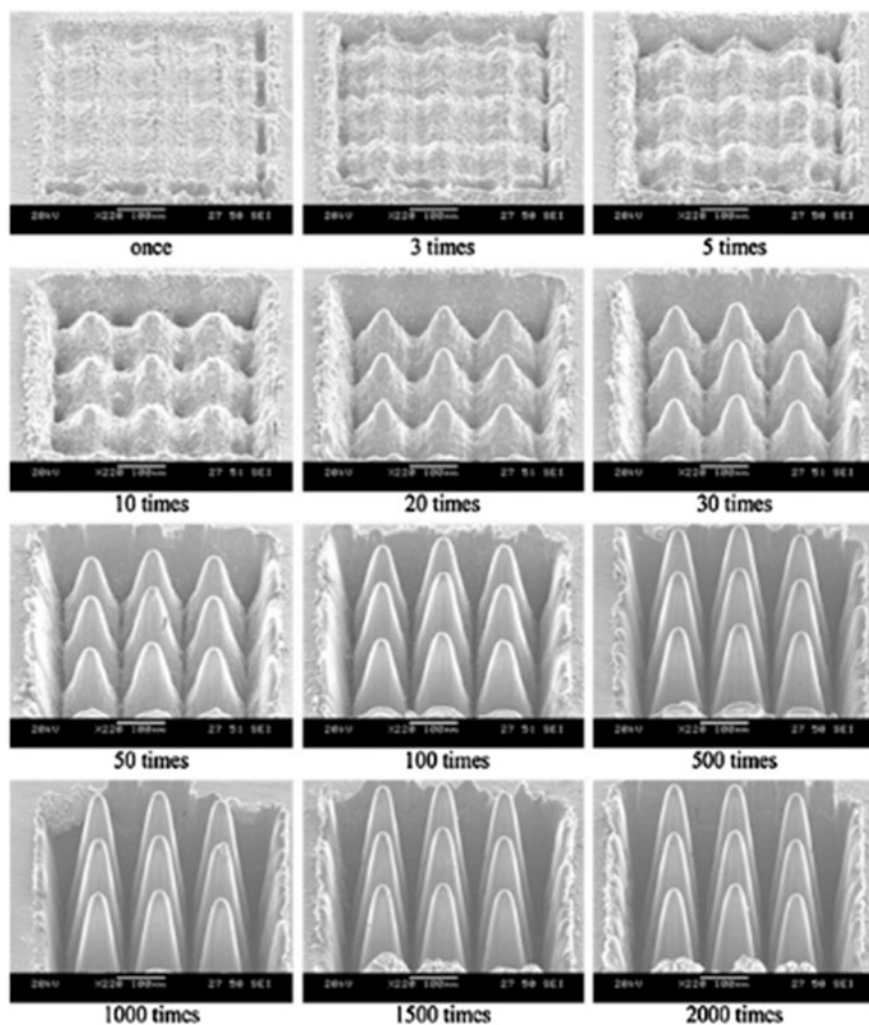


Fig. 3 Recast layer piling procedure according to the scanning repeat count [101]

2.4.1 Ablation Mechanism in Laser Beam Drilling

In principle, the ablation mechanism in drilling is more or less similar to the basic mechanism of laser beam milling. However, some differences are encountered if the aim is deep drilling or through drilling. When laser radiations strikes on the workpiece surface then absorption, reflection, refraction, scattering and transmission takes place which leads the complex understanding of the actual ablation phenomenon. Among others, the major phenomenon include melting, dissociation and evaporation processes. The dissociations or decompositions in metals and

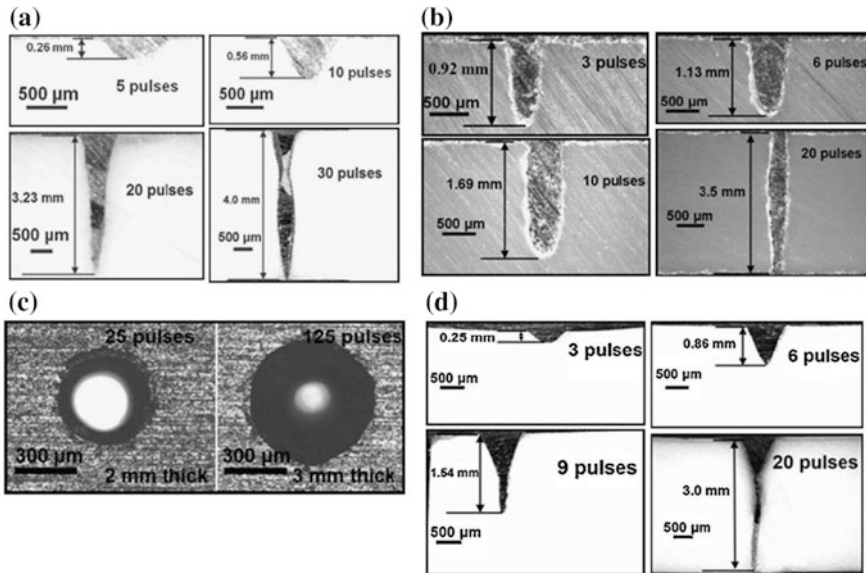


Fig. 4 Laser machining of **a** Al_2O_3 , **b** Si_3N_4 , **c** SiC and **d** MgO [102]

ceramics contains all the three material states; solid, liquid and gas. Vaporized material develops a vapor pressure, acting in upward direction, proportional to the laser fluence and inversely to machined depth. That is why for deep machining the material removal offers more resistance [102]. As ablation depends on the energy absorption which solely varies material to material [103], that's why the depth of machined feature does not remain same for even same class of materials and sometimes originates side [104] and interfacial cracking [105]. The mechanism becomes different if the target is through machining, especially when the ablation reaches near the bottom of the substrate. At this point another force (gravitational force of the melt) may come into place which causes the vaporized material to flow downside instead of moving upward [106].

2.4.2 Parametric Effects in Laser Beam Drilling

Range of laser types (CO_2 , Nd:YAG, Nd:YVO₄) are experienced for drilling metals but the pulsed Nd:YAG is the only type which is commonly employed for drilling of non-metals. High laser power (in kW) and high pulse frequency (1–250 kHz) is generally required for drilling process. However, low power can also be employed with other parametric adjustments. In terms of wavelength there is close match between metals and non-metals. However, pulse width is different for metals (5 ms–10 ns) than for non-metals (in Pico seconds). The recommended spot

diameter for metal drilling is 100–300 μm and nearly 30 μm for non-metals (referenced in below half of Table 1).

The main concerns in drilling is to achieve high aspect ratio, better circularity and low taper. However, in many applications taper less or reverse tapered hole is required. In connection to the laser power, assist gas pressure, number of pulses, pulse energy and standoff distance are the controllable parameters for the above said concerns. During deep hole drilling (25 mm thickness) of Inconel 718, five process parameters—pulse energy, pulse duration, pulse shape, focal position, and assist gas pressure—are crucial for hole quality [107]. Increase in power and number of pulses and assist gas pressure increase the depth of hole (Fig. 4) but insignificantly (20%) affect the taper and circularity in polymeric materials [102], nickel based alloys [71] and aluminum sheets [108]. However, laser power and assist gas severely affect the drilling of small holes (2 mm diameter) and deposit high spatter around the hole [109]. The size and temperature of the melt significantly affect the hole taper and spatter deposition [110]. But, the spatter can be minimized by some anti-spatter composite coating (ASCC) [111]. Standoff distance controls the taper and circularity but majorly (80%) contribute to the taperness [112]. Drilling quality is also very much sensitive to the consumption and flow of assist gas [113]. It directly affect the material removal capability [114], drilling speed [115] and the thermal distributions due to convective cooling by the assist gas [106]. Temperature and HAZ variations are different along the circumference than along the thickness. A handful FEA findings for metal drilling exists in literature to estimate thermal distributions and HAZ but for non-metals such modeling is not very common. Beno and Hulling [116] deduced a methodology for the temperature measurements at the edges (during cutting and drilling) of tool steel, aged Inconel 718 and Ti6Al4V. They employed two color fiber optic ratio pyrometer which has the benefit of measurement of temperature irrespective to the work material's emissivity. The emissivity depends only on the incident wavelength not to the temperature, direction or surface structure.

In much common practice scanning optics are utilized in laser drilling process. Scanning optics always shape a taper in drilled holes which is a universal problem of laser drilling. LMBT GmbH in Germany (working in the areas of Biomedical Optics and Applied Laser Technology) designed a patented device (in two models; 2.1 and 2.2) with rotating optics which can resolve this problem [117]. The device allows the beam to displace angularly at a controlled speed and inclination. They achieved even the reverse taper hole in stainless steel [118]. In a similar fashion, laser helical drilling can fulfil modern drilling requirements, in which laser beam rotates relative to work. The hole diameter in helical drilling is mainly the function of diameter of helical motion, but also influenced by pulse energy [119]. Man et al. [120] experienced a laser micro-drilling on titanium and TiN coated titanium. Because of the difference in melting points between the TiN and Ti phases, holes of different geometry were obtained. In the TiN coated titanium specimen vase shape holes were obtained. By applying the electrochemical dissolution technique, the vase shape holes were connected at the root of the holes and a subsurface porous network was formed. This structure is expected to enhance the fixation of dental implants [120].

2.5 Dual Beam Laser Machining

Traditionally the laser beam milling utilize single beam of laser in all of its process either it is cutting, milling, drilling or trepanning. Few of the researchers employed two types of laser beams to perform the same operations of laser beam milling as of single beam. One beam is normally defocused and the other is focused. In dual beam laser machining a focused CO_2 laser scribes the straight line whereas a defocused CO_2 laser beam (Fig. 5) irradiates on scribing line to induce thermal stresses and separates the material by fracture propagation. Defocused laser has the lower power densities and does not melt the surface but induce the steep thermal stresses during the cooling step. If thermal stresses are larger than the rupture strength, the fracture propagates along the scribing line and subsequently the material gets separated from the bulk [86]. The comparison between single laser beam and dual laser beam machining shows that dual laser offers less thermal stresses in final. It is suggested that if the distance between off-focus and focused beam is chosen close and close then the stresses can further be reduced [121]. The dual beam could be from two distinct sources or single beam splitting into two siblings by mirror reflection arrangements. Such arrangement is designed by [122] with the name of laser beam modulating device. The design consists of optical beam expander with a fast rotating beam chopper which splits the mother beam into two parts.

The dual beam concept is also applicable in fracture machining element technique in which the machining is carried out in the form of removal of series of predefined shaped elements. Laser beam focuses on the work to scribe a series of groove cracks. The defocused laser originates the tensile stresses concentrated at the tip of groove-crack and penetration of the existing crack further propagates. The material removal is thus the result of linkage of groove-cracks [123].

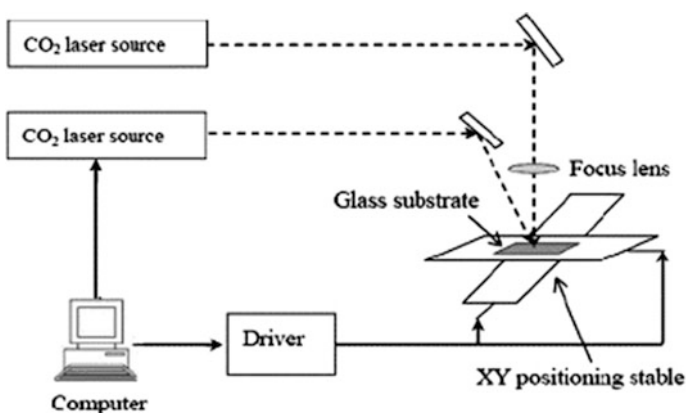


Fig. 5 Configuration of laser cutting system with the dual-laser-beam method [86]

2.6 Conclusions and Remarks

Laser beam milling is extensively used process that equally suits for metals and non-metals. Laser cutting, milling, trapenning and drilling are the famous processes. From the above discussion the following inferences could be realized:

1. There are many factors influencing the ablation mechanism. The driving forces for the ablation are still not well understood due to complex phenomenon occurring at machining zone.
2. The ablation mechanism is different for laser beam milling than drilling. There is also difference in mechanism for blind and through drilling.
3. Laser power, assist gas pressure, number of pulses, pulse energy and standoff distance are the governable parameters in laser beam drilling which directly influence the circularity and taperness of the drilled holes.
4. In terms of laser parameters, the only common difference in laser beam milling and laser beam drilling is the choice of laser power. Generally, high power lasers (in kW) are employed for laser beam drilling and low power (in hundreds of watt) for laser beam milling.
5. The commonly known problems of laser beam milling are low MRR, recast layer, delamination, thermal damage and HAZ.
 - (a) On the one opinion, these are controlled by tuning the wavelength, spot diameter and pulse frequency. Laser power also influence but generally low power (average power of 8–20 W) with relatively high pulse frequency (10–80 kHz) is suitable for LBM of metals and non-metals.
 - (b) On the other opinion, some auxiliary techniques (Grit blasting, laser-induced plasma micro-machining; LIPMM) along with laser irradiations show competitive results in terms of MRR, HAZ and cut quality.
6. Thermal stresses induced by laser heating is a prevalent problem of laser beam milling. The use of dual laser beam could be another alternative having the potential to reduce the thermal stresses.

3 Laser Assisted Machining (LAM)

LAM is a method of generally machining difficult to machine materials in which laser energy is used as an intense heating source while mechanical energy from some other process (planning, turning, milling etc.) is to remove the material. Laser energy thermally soften the material and cutting tool immediate behind the laser spot remove the material [126]. The material does not undergo any melting or evaporation state as in case of LBM. Indeed at the point of cutting, the high temperature generated by laser irradiations weakens the specific cutting energy which improves the machinability. For large number of materials the drop in materials strength occurs in between 500 to 600 °C [127].

3.1 Material Removal Mechanism in LAM

The LAM mechanism is very complex in nature due to the complexity of influencing parameters and their mutual interactions [128]. There are four types of parameters [127]:

- (a) Cutting parameters (speed, feed rate, depth of cut, type of tool etc.)
- (b) Tool parameters (tool type, side/rack angles, nose radius etc.)
- (c) Laser parameters (Power, repetition rate, pulse width, spot diameters etc.)
- (d) Interaction parameters (laser orientation, laser to tool distance etc.).

When work temperature increases the viscosity of the boundary particles decreases which enhance the plastic flow [126]. So, when the temperature reaches to the material's glassy phase transient temperature, the viscosity decreases and material lattice gets mobilized. The lattice begins to slip at its boundaries. The cutting forces by tool cause, later on, the plastic deformation and actual material removal [129]. The mechanism becomes little different when dealing with metal matrix composites. This is due to tool-particle interaction behavior. For example, TiC particle gets broken during LAM of matrix plastic deformation and embed into the matrix softened by LAM sponsorship [130].

Chip formation is essential element of LAM and depends on several factors. Chip quantity also increases by increasing the temperature [126]. Generally, the shape of chip formed in LAM is highly irregular patterned characterized by larger fluctuations in segment height. Increase in cutting speed results in thinner chips. However, in LAM of Nickel alloys continuous ribbon-like chips are found. LAM oriented chips show more tendency to shear localization and greater strain in the primary shear zone due to the thermal softening influence [131]. There are three softening mechanisms involved in this context [132].

- (a) Material yield strength reduction
- (b) Material base hardness reduction
- (c) Elimination of the work hardening.

3.2 Parametric Effects and Inspirations of LAM

Laser assistance is more widely practiced in conventional turning of hard-to-machine materials such as ceramics, hardened steels and metallic alloys (Nickel and Titanium). The turning process can be enriched in terms of tool life, cutting forces, material removal rates (MRR) and workpiece surface integrity (upper half of Table 2). However, during traditional milling and planing processes very few attempts are made regarding LAM. The focus is only converged to evaluate the reduction in cutting forces and HAZ (lower half of Table 2). There is very less attraction towards MRR and surface integrity.

Table 2 Inspirations of laser assisted machining (turning, milling and heating)

Process	Work material	Investigations	Machine	Tool	Laser type	Cutting force reduction	Increase in MRR	Surface roughness reduction	References
Laser assisted turning	Al ₂ O ₃	Cutting forces	FEMCO-CNC lathe	Cubic Boron Nitrides (CBN)	Pulsed Nd: YAG 60 W	15%	23.5 mm ³ /s	Oxide free layer	[129–131,
	Beta titanium alloy	MRR	Haifco Metal Master lathe	Tungsten Carbide (TC) Carbides	kW Nd:YAG	20–35%	20%	5%	133–135, 137,
Laser assisted milling/heating	AISI D2	Surface integrity	Turret lathe	Poly-Crystalline-Diamond (PCD)	1.5 kW CO ₂	15%	800%	15%	138, 140, 143,
	4140 steel	Tool life	3.5 hp lathe	SiAlON	2 kW HDPL	24%		25%	144, 149–151]
Laser assisted turning	AS2027 Grade	Microstructure	CNC turning center	PCBN	1.5 kW CW CO ₂	20%		30%	
	Ti MMCs		CNC lathe		Ytterbium fiber			Up to 0.3 µm	
Laser assisted milling/heating	Inconel 718							2.98 µm less	
	AISI 4130 steel								
Laser assisted turning	A2 tool steel	Tool wear	CNC Milling	TiAlN-coated tungsten carbide end mill	35 W CW Ytterbium doped	20% in sum	200%	2.98 µm less	[99, 126, 128,
	Ti6Al4V	Cutting forces	Machining center	Cubic Boron Nitride (CBN) end mill	1.5 kW CO ₂	25% in X			136, 141, 145,
Laser assisted milling/heating	Stainless steel	Surface integrity	Deckel Maho milling machine	TiAlN-coated carbide insert	Rofin-Sinar	60% in Y			146, 152, 153
	Mild steel	Thermal distribution			2.5 kW Nd: YAG	65% in Z-directions			
Laser assisted turning	Titanium alloy	Tool life			Rofin-Sinar CW CO ₂				
	Nickel alloy	MRR			6 kW Yb: YAG laser				
Laser assisted turning	H-13 steel	HAZ			CW CO ₂				
	100Cr6				25 W				
Laser assisted turning	Al ₂ O ₃								
	Mullite								

3.2.1 Cutting Forces and Material Removal Rate

Cutting forces increase with an increase in feed rate during conventional turning and obeys a linear relationship. But, during LAM, the cutting forces are always lower at all feed rates and cutting speeds (Fig. 6). It is interesting that during LAM the relationship also remains linear as the cutting forces depend upon the MRR. On average 12% forces can be reduced during LAM of titanium beta alloys [133]. Among others, laser power is the majorly influencing parameter for heating, cutting forces and MRR. High power ranges from 1.5–2.5 kW is mainly reported. The laser power of 400 W or below does not impart any reduction in cutting forces in comparison with CM [134]. The cutting forces encounters in different directions and components. LAM can reduce the cutting feed forces by 22% for ceramics [126] and hardened steels [135]. For titanium alloys, a reduction of force in X-direction up to 25%, Y-direction up to 60% and Z-direction up to 65% can be achieved [136]. In sum of all, LAM can ensure cutting forces reduction by up to 40% for different materials [127]. The cutting forces are commonly measured by dynamometer or three-component dynamic force sensor [137]. Kistler (model 9121 [130] and [138], 9255 [126]) dynamometer is proven to be good. A PCB Model 260A01 force sensor can be used to measure three dimensional forces [133] and [137]. Kim and Lee examined cutting force and preheating temperature predictions for laser-assisted milling of Inconel 718 and proved that its machinability can be enhanced by the reduction of cutting tool forces [139].

Reduction in cutting forces results in longer tooling life, high MRR and conclusively lowers the associated machining cost. LAM allows to achieve significantly high MRR in ceramics [129]. Hard to machine alloys (such as nickel based superalloys and titanium beta alloys) can even be machined with eight-fold high MRR via LAM [131, 133]. Due to lesser cutting forces, LAM can yield an overall

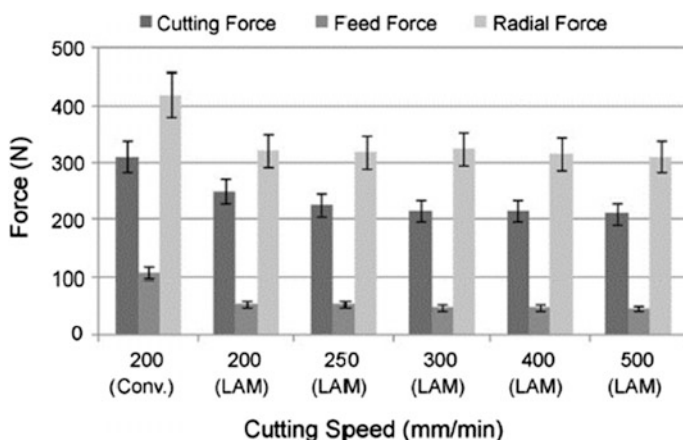


Fig. 6 Effect of cutting speed on cutting forces for conventional and LAM machining (feed = 0.25 mm/rev) [131]



Fig. 7 Damage in the cutting tool when the laser beam is focused at a circumferential distance of 25 mm from the cutting tool [132]

cost savings of 30% for titanium alloys [140] and about 20% of compacted graphite iron (CGI) [138]. To reduce machining forces by LAM it is believed that the laser spot has to be as near to the tool as possible. Heat penetration increases with the increase in laser spot-to-tool distance which offers more thermal softening [137]. However, the distance between the tool and the laser spot must be sufficient to prevent degradation of the tool (Fig. 7). There is a minimum distance (45 mm) to avoid tool degradation by overheating [132]. During turning of titanium beta alloys [133] suggest that 208 ± 75 mm distance is safer. In laser assisted milling the distance is taken from laser spot center to cutting tool axis and similar number (250 mm) is nominal [141].

3.2.2 Tool Life and Surface Roughness

Tool wear is the major factor that adversely affect the work surface. If the tool life is enhanced, the tool wear would be less and consequently the resulting surface roughness could relatively be improved [129]. Tool wear is found to be widely evaluated during LAM and is always less (Fig. 8) compared to CM. Most commonly used tools are tungsten carbide, cubic boron nitride (CBN) and (PCBN). The results express a mix of belief especially for surface finish. The reduction of the work hardening, by laser, leads to a lesser notch wear that limits the threat of abrupt failure of the tool and hence the wear mode change to flank wear, which results to a governable tool life and improved surface roughness [132]. Tool life (TC tools) can

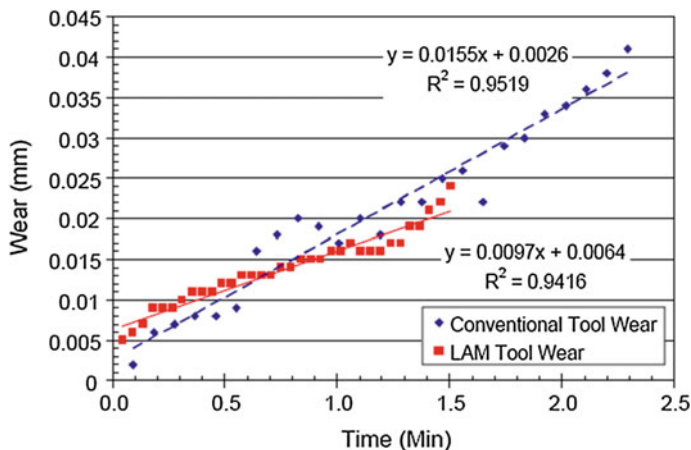


Fig. 8 Comparison of conventional and LAM tool wear [138]

be improved in a range of 60–100% for hardened steel [135] and CGI, respectively [138]. This improvement can be reached to 180% for PCD tool against composites [130]. For testing the tool wear, ISO3685 standard is a scientific choice. It states that the tool life is the time it takes for the average wear on the flank to reach 300 μm or until the maximum wear on any part of the flank reaches 600 μm , whichever occurs earlier. The standard is very rarely adopted. That is why the [142]’s findings show contradiction with the other results and stated that at 150–250 $^{\circ}\text{C}$ the tool life improves maximum to 7% but above this heating range, tool life shortened rather improvement.

On the other hand, laser assistance positively affect the surface finish. It allows to achieve surface finish of R_a less than 0.3 μm for hardened steel [143] and ceramics [126]. For nickel [131] and titanium alloys, the surface roughness can be improved up to 30% compare to conventional turning [140], however, very minor improvement (5%) is reported for graphite iron [138]. For white cast iron and composites, surface integrity results are reversed. Laser causes more frequent shearing of material, and surface profile results point to less uniformity [137]. In case of composites under LAM, roughness increases by 15%. These contradictory results could be due to difference of tool-particle interactions and chip formation mechanisms [130].

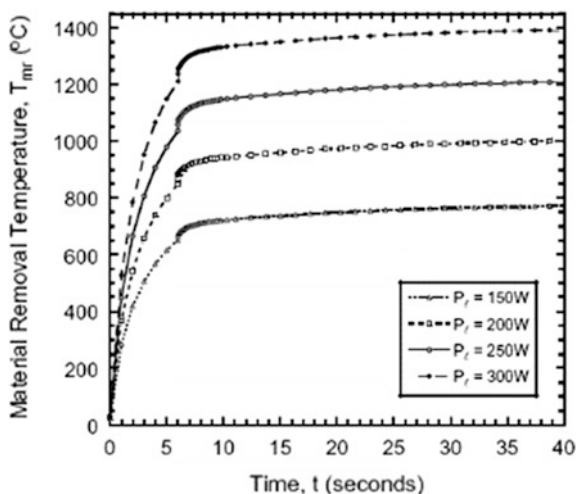
3.2.3 Temperature Fields Measurements and Microstructure

There are three kinds of temperature measurements and monitoring during LAM. To assure that the temperature reaches only the softening temperature, a static temperature measurement is essential [126]. Infrared thermometer or thermal camera [133] can be used to measure work surface and laser spot temperature [129].

Radiation pyrometer can also be used to record cutting zone temperatures [144]. Most widely used method of workpiece temperature measurement is the measurement via thermocouples (k or J type) [145, 146]. The micro thin film thermocouples (TFTCs) can be useful in measuring the transient temperatures at micrometers away from the laser–material interaction region on the workpiece [95]. The validation of thermocouple data can be calibrated by the study of [147]. These measurements can also theoretically be calculated by equations of transient heat transfer [137]. To predict the heat distributions, numerous techniques are seen such as Lattice Boltzman Method [126], solving heat equations [148], parabolic heat conduction equation etc. [129]. Though, the transient, 3-D model is widely attempted [149]. A 3-D transient thermal model can be used to estimate the laser parameters for certain cut quality that will yield no HAZ [145].

Temperature fields basically allows to understand the cutting force and residual stress phenomenon [127]. Laser power has strong effect on LAM obeying linear relationship with temperature variations (Fig. 9) [144]. Depth and width of HAZ increases with increase of laser power [148]. The optimum laser power density is important to achieve the desired surface heating otherwise greater power densities can cause the plasma generation and consequently damage the surface prior to actual cutting [131]. Chemical constituents of the surface generated by LAM remains almost unchanged [126, 138] and causes no difference in microstructure [140]. In general, the higher the laser power is higher the hardness is near the surface of workpiece. There appears to be no clear correlation between the depth of heat penetration and the hardness [137]. Micro-hardness shows that hardness is at maximum on the top surface and decreases towards bulk. At a depth of 150 μm the hardness approaches to that of bulk material [146]. The hard surface layer is the result of strain hardening under high pressure and temperature conditions (during

Fig. 9 Variation of material removal temperature with laser power [144]



heating and machining) and afterwards the cold working action when machined area rapidly cools down [131]. In general, LAM allows to achieve more uniform hardness and no microstructural change compare to conventional machining [143].

3.3 Conclusions and Remarks

The conventional machining processes especially turning and milling are aided by laser energy. The key motivation is to lower the workpiece hardness by softening the surface layers up to certain depth by laser heating. The vital conclusions which may arise by this section includes:

1. The laser energy positively influence the LAM processes in terms of reduction in cutting forces, increase in MRR, improvement in tool life and more shiningly the surface integrity.
2. Laser assisted turning is the most widely endeavored process as compared to laser assisted milling.
3. Compared to conventional machining, cutting forces are always lower during LAM at any feed rate value. On average, 15–35% of cutting forces can be reduced by laser assistance for both turning and milling processes.
4. Laser power plays important role in the reduction of cutting forces. High power ranges from 1.5–2.5 kW is mainly reported to reduce the yield strength of material. The laser power of 400 W or below does not impart any reduction in cutting forces in comparison with CM.
5. The distance of laser spot from cutting tool is very important to avoid the melting of tool tip. An average distance of 45 mm is considered as safe distance.
6. In almost all the cases the surface roughness produced by LAM is lower than that of CM. A 30% reduction in surface roughness can be achieved via LAM.
7. Overall tool wear is found to be less in LAM as compared to CM which leads to improve the tool life. However, very rare conflict is there that negates the improvements in tool life.
8. LAM is capable to induce more uniform surface hardness with no microstructural alterations than CM.

4 Laser Chemical Machining/Etching (LCM/E)

Direct laser ablation mainly removes material as vapor, hence, requires the delivery of a high power density within a very short interaction or pulse time. This leads to produce recast layers, burrs and melt droplets at the machining edge. For machining grooves even with pico-second or femto-second laser pulses this cannot be completely avoided. Laser chemical removal, that allows surface heating without surface melting or vaporizing, requires a low power density. Therefore, LBM's many

drawbacks (such as detrimental thermal effects, recast or re-deposition of evaporated material) can be avoided [154]. Laser thermochemical etching of metals can be achieved in solutions of acids using pulsed or continuous wave (CW) lasers. Compared to electrochemical machining (ECM), that also allows the processing of conductive materials regardless of their hardness [155], LCM/E's aspect ratio is much smaller [156] but it has good agreement with better resolution [157] and surface roughness [158]. In comparison to direct laser ablation the MRR and aspect ratio of LCM/E are smaller but it involves little heat generation [159] and thus thermal effects do not occur [160]. Due to the required low laser power density, melting is avoided, resulting in high-precision cutting edges without burrs and debris. Further, micro-cracks do not occur. Therefore, laser chemical etching is quite suitable for machining wide range of materials not only thick samples [161] but also thin foils [162] and even wafers with high precision and ultra-smooth surface with nm level roughness [163].

4.1 LCM/E Mechanism

The LCM/E mechanism is termed as the laser activated thermal-chemical mechanism [164]. Various phenomenon involves in LCM/E including laser energy absorption, chemical reaction, heat diffusion, hydrodynamics and mass transfer. Energy absorption, chemical reaction and mass transfer are mainly found in open literature that govern the etching performance.

Reduction oxidation reaction (Redox reaction) is the fundamental phenomenon of LCM. It is driven by the temperature dependent proton activity of a redox reaction. The laser energy just supports the kinematic of dissolution and has no melting effects. The radiation wavelength has an indirect impact by variances in absorptivity of the machined material, but no direct impact. Main ingredients influencing the surface temperature of the material are the laser power, laser wavelength and the spot diameter. In addition, reflectivity for a specific wavelength and the thermal conductivity are relevant material parameters that influence the surface temperature [165]. The processing speed is usually limited by the diffusion of anions formed during the redox reaction. The transport of reaction product is critical phenomenon that depends on the liquid viscosity and the diffusion coefficients. Stokes-Einstein equation helps to calculate these coefficients. Dynamic viscosity of the etchant also influences the process transportation. Arrhenius-Andrade equation simplifies the viscosity calculations. Method of etchant supply plays important role in material transportation. Commonly, a fixed quantity of etchant is provided in the horizontal positioned beaker that pose limitations. The circulation of etchant having certain flow rate could improve material ejection. Very sparse literature is available in this regard. Stephen and Vollertsen [165] injected the etching liquid (consisting of 5.6 M phosphoric acid and 1.5 M sulfuric acid) coaxially to the laser beam directly into the irradiated area in order to improve the material ejection during nickel processing. It was evidenced that the machining

quality with respect to aspect ratio, edge radius and roughness can be enhanced by increasing the velocity of the etching liquid. The etchant flow speeds ranging between 2 to 20 m/s offers competitive results. In another study the same author fabricated electron beam apertures and finishing of micro forming tools by LCM/E [160]. Li and Achara [166] achieved 300% high MRR for stainless steel using Nd: YVO₄ laser with 2.6 W and high repetition frequency of 25 kHz. They employed chloride solution with varying concentrations (5–75%). They fabricated groves and holes in 316 SS with comparably good precision, almost no HAZ and recast layer. The analysis depicted that the NaCl concentration of 50% could offer maximum grove depth. Very common phenomena of LCM/E is the boiling of etchant upon the laser irradiation. This leads to generate the bubbles and their entrapment at the machining zone. Dealing with these etchant bubbles and their further influences on the process throughput is very rarely attempted. According to [167], these bubbles reduces the MRR and etching performance and also cause the machining cavity to become irregular.

4.2 Parametric Effects and Inspirations of LCM/E

Formation of nano holes and other porous structures with very fine and regular porosity in thin metal sheets enable inventions or further developments of multitude of components such as substrate applications in fuel cell technology, microelectronics and catalytic reaction spaces in chemical reactors. Laser ablation assisted with chemical etching is promising technique to achieve such porous structures in wide variety of materials. 3D structures are also fabricated by some investigators through this technique even with high aspect ratio (~ 10). The process can be executed at room temperature or above depending upon the desired etch rate. The basic function of laser energy here is to make ground substrate ready for the initiation of chemical etching. The etching typically does not start until some pre-shapes are textured on work surface. Therefore, the top surface is modified by laser energy (known as photo-modification process [168]) to enable the reaction initiation [169]. Pre-holes, in common, are generated to start chemical etching.

4.2.1 Porous Structures

The laser fluence and wavelength are found as foremost parameters to control the etching performance and pore density. In order to achieve the porous layer a threshold fluence is necessary to supply. Less than this threshold there could not be any porous layer. Higher laser wavelengths give high etching perforce. Lin et al. [170] produced a large scale and highly dense nano-holes (Fig. 10) on stainless steel and titanium substrates by laser assisted hydrogen etching. The water was treated as etching liquid. It was found that the nano-hole density does not increase until recrystallization of the substructures is assured. This method is applicable for

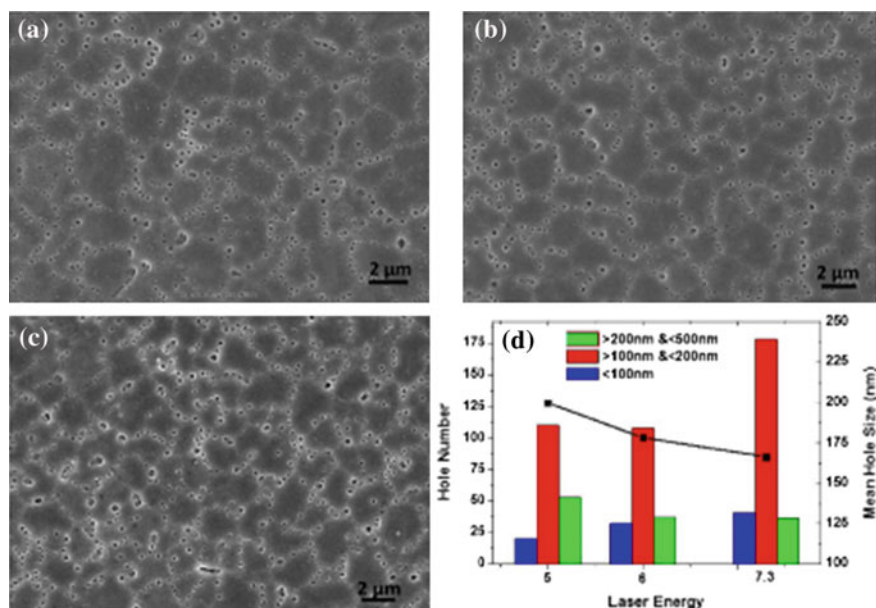


Fig. 10 Nano-holes. **a–c** Laser irradiation power 5, 6 and 7.3 W, respectively, **d** count of nano-hole size distribution and total number under different treatment conditions [170]

variety of materials such as Ni, NiTi, Cu₂O, etc. In the same line, N  th et al. [171] achieved nano-porous metal membrane with fine and regular porosity by the combination of the laser etching and electrochemical-etching techniques in nickel based superalloys. The synthesis of micro and nano porous structures with various morphologies is also supported by Al-Khazraji et al. [172]. In this study two types of lasers (CW diode and Q-switched Nd:YAG) with wide range of wavelength (405, 530, 650, 810 and 1060 nm) were applied under 30% diluted HF solution. High pore density with 3 μm pore diameter can be achieved in silicon wafer. The interesting thing is that the silicon wafer remains inert in HF until the presence of holes at the surface. The laser energy absorption induces holes to initiate the chemical reaction. It was found that longer laser wavelength has a higher etching rate and this could be recognized to the higher absorption coefficient. They reported that at low laser power density (<3 W/cm²) no porous layer was observed. Whereas, the etching rate rises to about three times when the laser power increases to 20 W/cm². Kumar et al. [173] also reported the surface morphologies of laser-etched silicon as a function of the laser power densities. They used four laser power densities (0.44, 0.88, 1.76 and 4.40 kW/cm²) and found that cracks were formed at very low power density and pillar like structures were shaped at very high laser power density. Therefore, to achieve the porous structure the laser fluence should neither be too low nor be too high. Nayak et al. [174] reported the same pillar like structures in silicon and germanium surfaces. Rather than liquid, they

prepared a gaseous etching environments of sulfur hexafluoride (SF₆) and hydrogen chloride (HCl). Conical shaped pillars with spike top and bulb-like top can be observed in germanium and silicon respectively. Under same processing conditions, the aspect ratio of silicon appeared to be higher than that of germanium.

4.2.2 3D Structures

LCM/E is considered as rapid and direct method for the fabrication of 3D and other periodic structures with fine surface roughness (~ 20 nm-Ra). The 3D fabrication involves a suitable combination of laser and etchant parameters simultaneously. This includes particularly laser power, repetition rate, scan speed, etchant concentration and processing time. According to [175], the average surface roughness (of micro trenches) is inversely proportional to scan speed and directly to laser repetition rate. The narrow laser spot size is good to achieve sharp sidewall and small HAZ. Zhang et al. [176] observed crack free side wall of Al₂O₃ during UV laser ablation and post processing chemical etching. High laser repetition rate with low power was recommended to achieve sidewall roughness of Ra 0.16 μ m. Zimmer et al. [177] studied the influence of laser fluence, pulse number and pulse length of Nd:YAG laser on etch rate and surface topography of fused silica. The results exhibited that the etch rate upswings linearly with the laser fluence and pulse length. The etched surfaces featured smooth, no ridge, re-deposited material or debris. Oh et al. [178] evaluated the sidewall roughness on SS foil (AISI 304, 500 μ m thickness) using two types of lasers (Nd:YAG and CW Nd:YVO₄) and 10% phosphoric acid as etchant. It is stated that depending upon whether a pulsed or a continuous wave (CW) laser is employed, the etch depth and surface morphology of the grooves varies significantly. Pulsed etching produces deep but rough microgrooves whereas CW etching results into shallow but smooth sidewall. To overcome the restrictions of both processes they developed a hybrid pulse-and-CW scanning process generating deep microgrooves with smooth sidewalls.

Luo and Tsai [169] fabricated an array of square columns (Fig. 11) with high aspect ratio (~ 10) on quartz glass by femtosecond laser inner modification. They employed 15 wt% hydrofluoric acid (HF) for 15 min as etching agent. In another study they achieved a 3D piled-octahedron structure by 5 wt% HF using very low power laser (100 mW) with high repetition rate (100 kHz). However, they applied femtosecond laser for embedded grating alone and then performed the etching in separate bath. It should be noted that the intrinsic quartz doesn't react with HF similar to silicon wafer (as mentioned before). In a similar study with nearly same fundamental parameters, they also optimized the laser power and aspect ratio for the fabrication of micro-lens array [179] and V-shaped micro prism [180]. But in general, the 3D pattern's pitch and aspect ratio is mainly controlled by etching concentration and processing time. Matsuo et al. [168] fabricated various kinds of micro-channels in Pyrex glass under femtosecond laser assisted etching with the use of aqueous solution of 10 mol/dm³ KOH. They experienced the etching at elevated

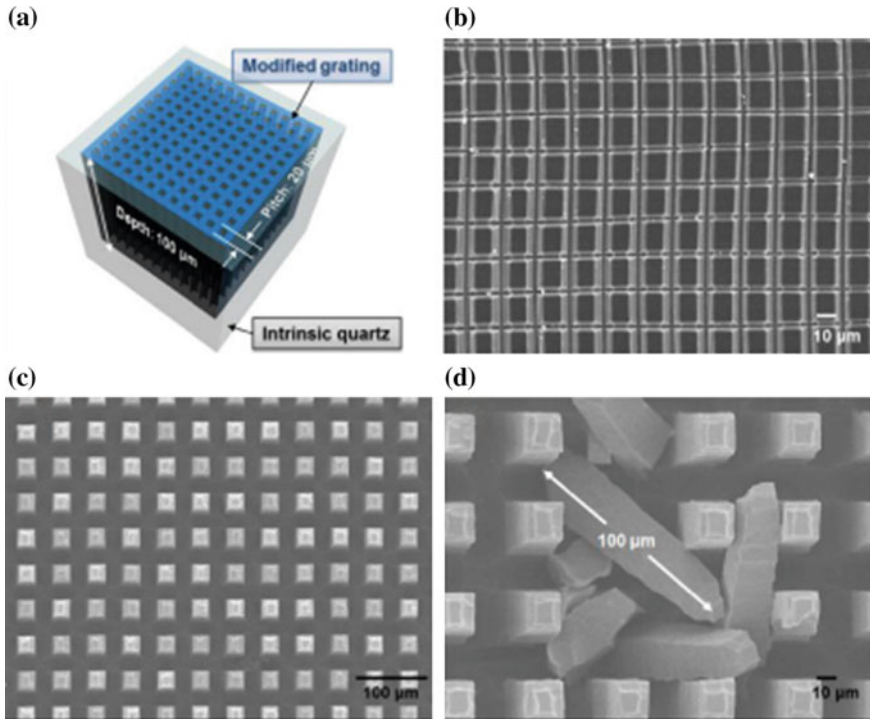


Fig. 11 Fabrication of grid photonic crystal structures inside quartz: **a** schematic diagram of the scanning pattern, **b**, **c** are SEM images of photonic structures, **d** SEM image of columns with high aspect ratio [169]

temperature (80 °C) instead of room temperature. The results seems to be similar as of other researchers' particularly in terms of laser parameters. The maximum etching rate recorded roughly 4 μm/min.

4.3 Conclusions and Remarks

The investigational outcomes discussed in this section has demonstrated that LCM/E is a potential candidate of machining processes to achieve high precision edges with nm level surface roughness for variety of materials. The conclusions that can easily be drawn by this section are:

1. Individually compared to ECM and LBM, this hybrid process is much superior in terms of surface morphologies, thermal damages, burrs free and re-deposited layers.
2. The machined feature and surface integrity depends on type of etchant and its flow speed.

3. It is proven as highly promising technique to fabricate 3D structure as well as micro-sized arrays.
4. In terms of synthesizing the porous structures for various applications, LCM/E is a competent alternative.
5. Other than positive aspects, there are two common drawbacks of LCM/E. It offers low MRR and short aspect ratio of machined cavities. Very rare in literature, high aspect ratio is achieved by this technique.
6. The major phenomena in LCM/E is the etching of substrate by chemical constituents through well-known redox reaction. The laser energy just prepares the target surface to initiate the chemical etching. That's why the MRR is low.

5 Laser Assisted Electrochemical Machining (LAECM)

There are two common etching techniques named as dry etching and wet etching. In dry etching, the material is etched/dissolved by reactive ions or vapor phase etchant. The ions are sputtered on material to execute physical knocking of atoms as well as chemical reaction. On the other hand, wet etching requires a work sample to be immersed in chemical solution (electrolyte) and chemically dissolves the material constituents by redox reaction. Both the techniques are good for micro-pattern and microstructure fabrication on various materials [181].

LAECM process is considered as one of the wet etching processes and is bit similar to LCM/E. The only difference is the chemical which is an electrolyte of certain salt solutions. The schematic diagram (Fig. 12) shows the role of both electrolyte and laser beam. The function of laser energy is to localize the machining zone and activate the target surface for chemical dissolution (similar to LCM/E) while electrolyte performs function of material dissolution, cooling and transportation of debris. Electrolyte reacts with the material but the role of laser energy is also found to be dominant by some researchers. The process is not much widely employed as per open available literature. But it offers much improved results in terms of material removal rate, surface finish, machining quality and dry laser defects. Figure 13a, b shows the micro-patterns fabricated by LAECM. Electrochemical machining (ECM) is a famous type of wet etching that is carried out, in general, in conjunction with photo-mask or micro-tool [182]. It enables to achieve microfabrication with minimal dimensional and thermal damage. In [183], N. Kasashima and T. Kurita successfully fabricated micro stent (used in medical implants) as shown in Fig. 13c, d, having outside and inside diameters of 210 and 100 μm respectively that is still a challenge for other processes.

Long et al. [185] compared the dry laser and LAECM characteristics for silicon wafer. The low power excimer laser with varying pulse frequency was applied under 20% KOH electrolyte with 1 mm layer thickness above work surface. It was found that the etching rate and surface finish are significantly high for LAECM compare to laser dry etching. In this compound process the laser interaction is

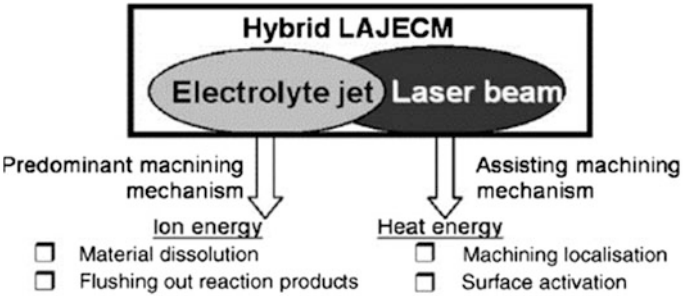


Fig. 12 Roles of electrolyte jet and laser in LAJECM [184]

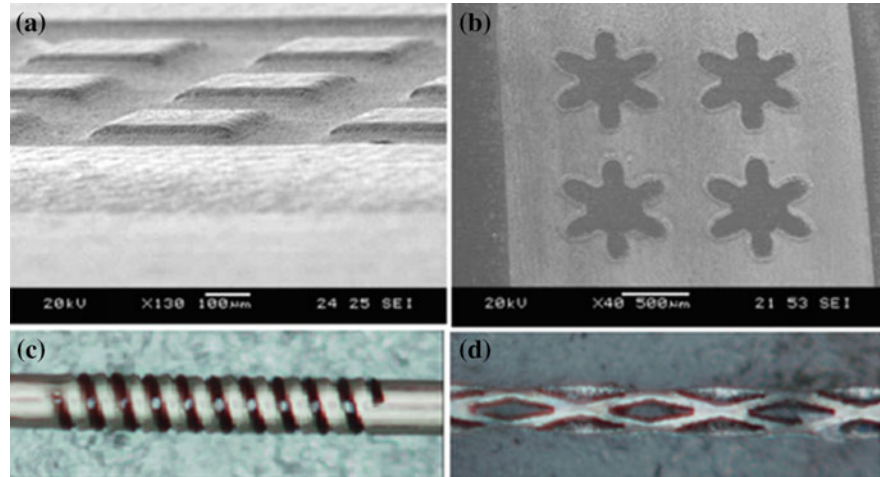


Fig. 13 Microfabrication by LAECM; **a, b** micro-patterns [181], **c, d** micro-stent with outside and inside diameters of 210 and 100 µm, respectively [183]

reported as the dominant factor for etching. Kikuchi et al. [186] fabricated micro-lens array of anodic alumina by Nd:YAG laser and electrochemical techniques (anodizing, electroplating, oxidation). They used a very low power laser (0.5–1.0 mW) having pulse width of 8 ns and 10 Hz repetition rate. A novel process for electrochemical etching of metal without a need for photo-mask is proposed by Shinet al. [187] termed as Electrochemical Etching using Laser Masking (EELM). This process executes in two steps; laser masking and anodic dissolution. In the laser masking step, a patterned layer on conductive layer is formed by laser marking using a pulsed fiber laser. The laser marked area temporarily inactive and serves as protective mask. Afterwards, this patterned surface selectively dissolves during the electrochemical etching step. A protective layer on surface is formed by laser marking, which is based on direct writing with a laser beam. The anodic dissolution rate of the unmarked area was substantially higher

than that of the laser marked area. One year later the same team investigated the changes in characteristics of recast layer formation and the protective effect of the recast layer according to the laser masking conditions and electrochemical etching conditions [188].

Fabrication of holes by laser drilling, especially in metals, exhibits recast layer and spatter around the periphery of the drilled hole. In order to avoid these potential problems, [189] proposed a hybrid process of laser drilling assisted with jet electrochemical machining (JECM-LD). In addition to cool down the work surface and transport the debris away, jet electrolyte also reacts with material. The shape of the drilled holes can be explored prior to actual drilling by 2D model presented in [190]. Drilling analysis of 321S20 stainless steel holes reveals that the laser energy (photon energy) is the main driving force while jet electrolyte (ion energy) reduces the drilling defects. In this connection De Silva et al. [191] reported that the role of laser in LAECM is to localize the machining area. The thermal enhancement of electrochemical enables the intensification of anodic dissolution that consequently raise the MRR and machining precision. Temperature is the predominant determinant and it must be controlled to avoid spark generation due to electrolyte boiling. They developed FE modelling for temperature field distributions for various alloys including stainless steel, aluminum alloy, hastelloy and titanium alloy. It was found that the modeling requires number of assumptions due to electrolyte flow, boiling, sparking, specimen shape, energy absorption and scattering etc. The dissolution mechanism mainly depends on material's properties. That's why the surface analysis showed variations for different materials. Under same conditions, Hastelloy exposed lowest surface roughness while titanium alloy showed highest reduction in taper (65%) [184]. According to [192] the MRR of LAECM is found to be linearly dependent on electrolyte concentration and jet velocity irrespective to the material type.

5.1 Conclusions and Remarks

Very less amount of research has been found under the category of LAECM. However, this hybrid process also has the potential to yield better results as compared to dry laser ablation. The MRR has been found to be more in the presence of electrolyte. The machined cavity or drilled holes through LAECM exhibit low machining defects as compared to dry laser machining.

6 Under-Water Laser Ablation (UWLA)

The hybrid laser-water technology is getting popular in order to achieve minimal thermal damages and improved MRR. Underwater laser processing provides a solution to the majority of the problems of laser machining in air and other gases

especially HAZ which can be substantially avoided due to the additional cooling action of water layer/jet [193]. A massive research is available in literature attempting underwater laser processing in order to alleviate the defects around the laser cut grooves and holes. It is also widely attempted to fabricate nano particles (discussed in next section) from variety of materials solid [194]. Several types of lasers (the same as used for dry LBM) are experimented in this regime including femtosecond, nanosecond, CO₂, Excimer and Nd:YAG laser. The crucial matter is to solely set an appropriate wavelength, pulse number, fluence, spot diameter and water film parameters to reach the desired ablation outcomes.

6.1 UWLA Mechanism

In UWLA or laser-water jet ablation the actual machining is caused by laser energy. The function of water is to restrict the realization of undesired defects like HAZ, recast layer, spatter and cracks etc. Therefore, unlike the LAECM, the occurrence of these defects still exists in the presence of water but at low level. The material removal mainly depends on laser parameters (especially spot diameter and the focal distance) and the fluid dynamics (particularly fluid layer thickness). However, the configuration of target material with respect to incident laser beam influences the ablation performance.

6.1.1 Beam Focus

As the sample is immersed in water, so, if the laser spot is focused on work surface the majority of the energy will be absorbed by water instead of work sample. It boils up and evaporates the water. This explosive evaporation of water molecules generate forces between substrate and the suspended melt particles. These forces are generally larger than adhesion forces thus propel the melt particles off the surface of material [195]. Thus the mechanism changes from thermal phenomena in air to a more mechanical in water. Therefore, in general, the best practice is to focus the laser beam below the work surface rather than focusing on top surface. It will bypass the high proportion of liquid layer to get boiled and impart maximum energy to the work material.

6.1.2 Water Layer Thickness

The water layer thickness above work surface plays important role in the ablation mechanism. It mainly decides the machined depth and kerf width [196]. The thick water layer carries away the debris more efficiently but also reduces the ablation rate. When the laser beam travels through thick liquid film, the pulse shape doesn't remain uniform and/or consistent. At the laser-work interface the formation of milky

suspension composed of liquid, bubbles and melt is formed that confines the plasma above target material. It scatters the laser light along with a distortion of the laser pulse and consequently the energy needs to ablate the material severely affects. High proportion of energy is absorbed by thick water film and thus attenuates the amount of energy to be absorbed by work material leading to less ablation efficiency [197]. Typical water layer thickness in horizontal position is 1–2 mm [198], however, different authors experienced different thickness values like [199] maintained 6 mm layer, [200, 201] worked at 1–20 mm layer. Similarly, to ensure handful rise of ablation rate, [196] suggested 3–4 mm layer thickness for alumina. The sprayed water in the form of thin layer could be an alternative solution to this problem [202]. On the other hand, as the energy absorbance depends on the material wavelength, therefore, the selection of incident laser wavelength, preferably, be such that it should strongly be absorbed by the target matter rather than water film. Based on this statement, Dupont et al. [195] claimed that a high ablation rate (2–15 times) for high laser intensities can be achieved if the laser wavelength is chosen in accordance with work material's wavelength. It has been proved that the energy absorbance doesn't depend on layer thickness but the incident light wavelength.

6.1.3 Splashing and Cavitation Bubbles

The water splashing and rise of temperature within the closed premises of laser beam are common phenomenon [203]. The splashing generates non-uniformity of the layer while rise of temperature leads to ineffective cooling mechanism. A closed flowing water immersion technique ensures a controlled geometry for both the optical interfaces of the flowing liquid film and permits repeatable control of flow-rate during machining. The splashes could somewhat be minimized due to flowing streams. In this way, however, the flow rate has its own implications and effects on precision and quality. Formation and diffusion of cavitation bubbles is another concrete phenomena of UWLA. That's why the morphological features of UWLA machined geometries differ. These features mainly attributes by laser pulses (N) per spot and the fluence level (F). The feature differences become more evident at high pulses per spot (100–1000 pulses). Different colored lights can be observed at different E or N values. For example, reddish light is produced in the laser-work-interface at low E or N values while a brilliant white light can be seen at high values. This is called confinement effect that is typically enhanced by liquid environment. It results a negligible amount of melt's re-deposition but lowers the ablation rate [204].

6.1.4 Melt Ejection and Sample Configuration

The convection induced fluid motion can also be observed during under water laser processing. It helps in the transportation of debris away from the material surface. The melt ejection may also be improved by changing sample configuration from

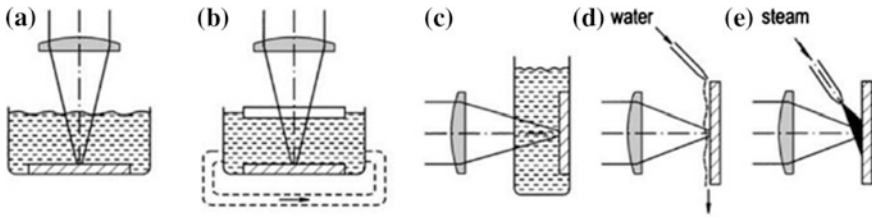


Fig. 14 Various methods for providing water at laser-material interaction zone [206]

horizontal to vertical (shown in Fig. 14) and laser from vertical to horizontal. In this way gravitational effect also adds up with fluid flow. The gravitational force itself drops down the melt debris and fluid stream that further improve the melt ejection phenomena. Even though, thin water film could easily be maintained by this orientation. In this way the ablation efficiency is much high than in horizontal position [205].

6.2 Parametric Effects of UWLA

Laser ablation under water is dealt with wide range of materials in literature including metals, alloys, ceramics, glass, polymers, semiconductors and many others. The effectual material removal by laser irradiations is a fundamental concern in micromachining. The research show that the water environment is a great candidate for material removal by laser especially where coarse removal is required. Ablated surface attributes, geometrical aspects (width, depth and aspect ratio), melt re-deposition and HAZ are generally evaluated and compared with laser ablation in air. Nevertheless the investigations of the ablation rate is a highly common attribute. The results are entirely based on the material and the laser-water parameter settings mainly; laser fluence, pulse numbers, repetition rate, spot diameter and water layer thickness. That's why the results are not consistent in literature especially for ablation rate. Both the high ablation and low ablation rates can be found in literature (as shown in Table 3). There are also certain materials, such as ceramics, having explicit behaviors among which thermal properties and brittleness are dominant. Such behaviors/materials leads the ablation mechanism somewhat away from the traditional ablation mechanism [207]. These behaviors are not discriminately addressed in open literature except few like exceptional behavior of Al_2O_3 : lower etching rate, greater surface coarseness and porosity, and lesser bending strength after laser ablation in water [200, 208].

Table 3 Ablation rate variations of different materials through UWLA

Ablation	Work material	Experimental conditions	Work position	Results	References
High ablation	• Aluminum	Pulse energy: 0–10 mJ Spot size: 10 μm Fluence: 127 J/cm ²	Horizontal	Etch grooves deeper in water than in air	[213]
	• Polyimide	Pulse duration: 20 ns Wavelength: 308 nm Fluence: <20 J/cm ²	Horizontal	Etching rate nearly same in water and air	[70]
	• Silicon	Fluence: 0–5 J/cm ² Wavelength: 780 Pulse repetition rate: 1 kHz	Horizontal	Etching rate two times in water than in air High aspect drilling was achieved	[209, 214]
	• Steel • Al ₂ O ₃ • SiO ₂	Fluence: 0.1–30 J/cm ² Spot diameter: 0.5 mm Water layer: 3–4 mm	Vertical Horizontal	Etch rate 2–15 times more in water than in air Recast layer and thermal damage was eliminated	[195, 196]
	• Al ₂ O ₃ • Porous MgO	Wavelength 308 nm, max. pulse energy 2 J, pulse duration 50 ns, Pulse repetition rate 20 Hz) Fluence: 0–35 J/cm ² Water layer: 1–20 mm	Vertical/horizontal	Etching rate is high in water than in air. The surface of Al ₂ O ₃ remained rough and porous	[200, 201]
Low ablation	• • Aluminum • Brass	Wavelength: 1064 nm Pulse width: 8 ns Pulse energy: 600 mJ Pulse repetition rate: 10 Hz	Vertical	Crater depth is more in water than in air	[207]
	• ZrO ₂ • SiC • Si ₃ N ₄ • Glass, • Stainless steel	Wavelength: 308 nm Maximum pulse energy: 2 J Pulse duration: 50 ns Pulse repetition rate: 20 Hz Fluence: 0–35 J/cm ²	Vertical/horizontal	Etching rate is low in water than in air	[200, 201]

(continued)

Table 3 (continued)

Ablation	Work material	Experimental conditions	Work position	Results	References
	<ul style="list-style-type: none">• Polyamide• Magnetic materials (NdFeB, ferrite)	Water layer: 1–20 mm Wavelength: 1.06 μm Pulse duration: 180 ns Pulse repetition rate: 1 kHz Water layer: 6 mm	Horizontal	Best surface finish and elimination of debris than in air. 2.5 times low ablation rate in water than in air	[199]
	<ul style="list-style-type: none">• Silicon	Pulse duration: 25 ns Wavelength: 248 nm Pulse repetition rate: 10 Hz Number of pulses: 10–5000 Laser energy: 100–480 mJ	Horizontal	Machined surface is rough under water and smooth in air	[197]
	<ul style="list-style-type: none">• Silicon wafer• Polycarbonate• SiC	Wavelength: 800 nm Pulse repetition rate: 1–1000 Hz	Vertical/horizontal	–	[204, 212]

6.2.1 High Ablation Rate

Normally, for high ablation rate with UWLA the low laser power (some watts) and low-to-medium fluence range ($0.1\text{--}30\text{ J/cm}^2$) are more practical. In the meantime, pulses need to be short (in μs or ns) and their frequency low ($<\text{kHz}$) in order to achieve high ablation rate. The authors of [198] perceived high ablation in water than in air for SiC at laser beam diameter of $20\text{ }\mu\text{m}$, pulse duration of 15 ns , fluence level of 16 J/cm^2 . However, they used a repetition rate of 8 kHz which is contradictory for high ablation rate as mentioned before. The reason of this high repetition was neither presented nor evaluated for any effect.

M. Geiger et al. [200] processed different ceramics (Al_2O_3 , MgO , SiC , ZrO_2 , Si_3N_4) under water at two work configurations (Horizontal and vertical). In horizontal position they employed $1\text{--}20\text{ mm}$ water level while in vertical state 2 mm thin layer. Mix of results were obtained for above materials. Al_2O_3 and MgO exhibited high ablation rate ($2\text{ }\mu\text{m/pulse}$) while in contrast to that the other materials showed slightly low ablation arte in water compared to in air. The ablation was, however, highest for both the vertical configuration having sprayed water technique and horizontal with 2 mm water level. With even 10 mm water level the ablation rate was significantly high. This is totally contradicting our prior discussion of proceeding section. They reasoned that the water level (up to some extent) doesn't lowers the laser energy and ablation rate if suitable laser wavelength is chosen. As the absorption coefficient of liquid varies with the radiation wavelength. So, they adjust the XeCl excimer laser's wavelength to 308 nm to which distilled water has low absorption coefficient. In a study of [209] the authors used 248 nm wavelength KrF excimer laser to ablate Si wafer under water thickness of 1 mm and reported the similar results. Likewise, the high ablation rate validations can be found in [195] for stainless steel, alumina, silica and in [201] for glass, stainless steel and polymers with steady results.

6.2.2 Low Ablation Rate

Some of the research portrayed the low ablation rate by UWLA as compared to dry conditions. Choo et al. [197] fabricated holes in Si. The results revealed that the ablation depth is mainly dependent on number of pulses and the fluence level. They reported threshold fluence of 2 J/cm^2 under water processing and 1.7 J/cm^2 for air. It means that the ablation depth is low by UWLA compared to dry ablation at certain fluence level. The experiments in [204] also exhibited almost same results for Si wafer under very similar conditions. The only difference was the value of wavelength and repetition rate (800 nm and $1\text{--}1000\text{ Hz}$ by [204] while 248 nm and 10 Hz by [197]). All this is the story of water at still level. The water flowing at some flow rate in a closed flow is another scheme mainly apply to enhance the melt removal. But this technique also lowers the ablation rate. However, the ablation threshold in flowing water is somewhat lower as compared to water at still level. To investigate the impact of this technique on ablation threshold, Dowding and

Lawrence [210] machined polycarbonate samples under various flow-rates. An average decrease in ablation threshold of 7.5% can be acquired using turbulent flow velocity regime while laminar flow gives negligible reduction. On the other hand, flow velocity of 3 m/s yields a minimum ablation threshold (112 mJ/cm^2).

6.2.3 Possible Reasons of Ablation Rate Variations

The above discussion reveals that the variation in ablation rate is a fact of UWLA, either positively or negatively. Few of the possible reasons of why ablation rate varies/differs in water and air could be:

- In liquids, the temperature of confined plasma remains higher than in air [209], thus the liquid prevents the plasma expansion [211] that enrich the laser radiation energy [198] and consequently improves etching rate [212].
- The shock wave generation, originating from plasma expansion and the collisions of vapor bubbles, produce the micro-jets. These micro-jets destroys the substrate surface (especially oxide layer) [200], that results high ablation rate in water [198].
- The projected shock pressure in water and air environment are $\sim 3 \text{ GPa}$ and $\sim 95 \text{ MPa}$, which means high pressure by water produces shock waves that lower the viscosity of molten material. Thus efficient material removal and ejection rate [207].
- The micro-bubbles carry the melt debris away more efficiently [213] that speeds up the ablation process.
- The vaporized bubbles and melt suspension scatter the laser light that lowers the machining rate in liquid.
- The water flowing direction influences the material ejection [206]. The vertically flowing water (Fig. 14d, e) assists the debris removal by its flow and gravitational effect that yields high ablation phenomena [205].
- Liquid layer thickness absorbs the high proportion of laser energy and attenuates the energy transmitted to target surface. This lowers the ablation efficiency [197].
- Liquid's absorption coefficient depending on laser wavelength creates the difference in ablation rate [200]. Low absorption coefficient enhances the ablation performance and vice versa [209].
- Differences in ablation also occurs due to material's inherent properties. For same laser-water parametric conditions some materials give high ablation [200] while some materials low ablation than in air [201].

6.3 Inspirations of UWLA

Cutting, surface craters, high aspect drilling and cavity machining are the main ablation processes performed by various researchers through UWLA. The main

focus in these processes is converged to study the process capabilities in terms of thermal effects, surface quality, re-deposition, micro-structural alterations and material removal.

6.3.1 Crater Formation and Structure Characteristics

The liquid environment in laser ablation has the advantage of completely preventing charring and reduction of spatter [206] and re-deposition of melt that in combine leads to good quality microstructures [201]. The suitable pulse duration and pulse frequency is considered as necessary to avoid microstructural defects. For example, pulses over 100 μs length could not eliminate recast layer in ceramics [215]. At further long pulse length (1 ms) and high repetition rate (over 50 kHz) the machined cavity gets wider and shallower. The recast layer is due to the re-deposition of melt particles which solidifies on the surface. This abundance of re-deposition is more in air than in water. But it can't entirely be eliminated even by UWLA. The size of re-deposited particles and their distribution across the crater periphery is significantly less in the presence of water than dry conditions. The experiments of [207] carried out on aluminum and brass samples by Nd:YAG laser with varying laser pulse energy under dry and wet conditions. The re-deposited particles to the material surface itself was found in both the ambient. The air atmosphere generates average particle size of 3 μm while in water the average size of re-deposited particles was 55 nm. The particle size is larger near the periphery than those away from edge. High intensities laser pulses are capable to generate a shallow crater when irradiating metal targets. Mahdiah et al. [216] worked on crater formation in aluminum target under dry laser and wet (water) laser conditions as presented in Fig. 15. According to their research findings the crater geometry extremely depends on the laser pulse intensity, the number of laser pulses and the ambient. Higher is the pulse numbers deeper and bigger is the creator. Similarly crater depth is linearly proportional to the pulse energy. The crater depth in water dramatically rise which strengthen the high ablation claims of UWLA. The same results are proofed for brass and aluminum by [207]. In addition to crater formation the presence of water also allows to generate nano-structures. These nano-structures can be characterized in various ways. The formation of such nano-structures is solely due to the re-deposition of ablated melt around the crater periphery. Figure 16 represent the needle-like nano-structures produced on brass target while crater formation through under-water laser machining.

6.3.2 Under-Water Laser Milling

Laser ablation in the presence of water is equally suited to mill three dimensional geometries in almost all kinds of materials either it is metal or non-metal. Similar to other advantages and applications it is greatly applied to achieve good geometrical precisions, surface quality, elimination of melt re-deposition and less thermal

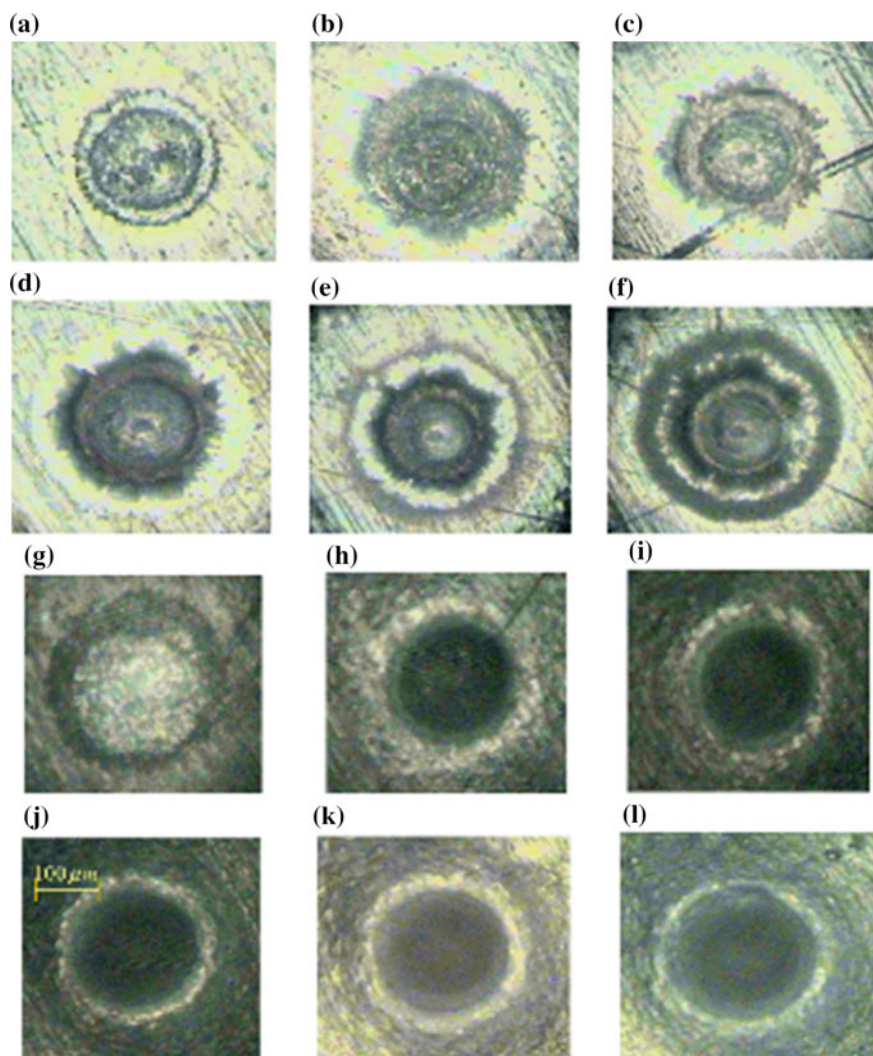
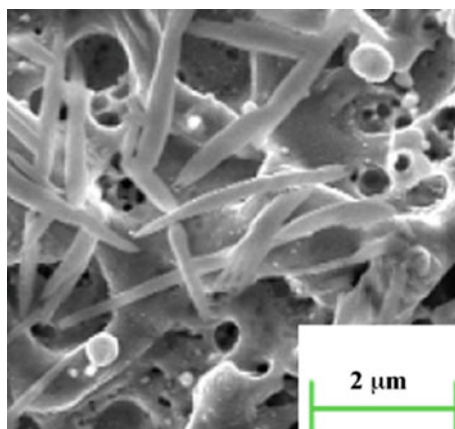


Fig. 15 Typical image of craters on an aluminum 5052 irradiated in air (*top*) and tap water (*bottom*) by different pulses [216]

damage. The experiments in [198] indicated that the precision and quality of machined cavity in SiC ceramics were high by under-water laser milling compared to milling in air. They also reported that the cavity surface was free of any visible layer of oxides. The laser machining of magnetic materials (NdFeB and ferrite) under water found to give much best surface finish and elimination of debris than in air [199]. Three dimensional cavities, holes and micro-channels have also been achieved in the water ambient by [217]. They employed the water jet on the rear side of the workpiece instead of traditional means of liquid supply on top surface.

Fig. 16 SEM image of the nano-structures at the crater periphery re-deposited on brass target in water [207]



CO₂ laser underwater machining has been found by Yan et al. [196] to result in reducing defects such as recast layer, dross, cracking and heat damages during the deep cavity machining of alumina. Different polygon cavities machined by underwater laser ablation are presented in Fig. 17.

The prediction of temperature field, stress field and material removal were realized by numerical and thermal models. The results showed a great agreement for all the characteristics. Afterwards, they achieved deep cavities with various shapes such as square cavity, circular cavity, triangular cavity, pentagon cavity and prismatic cavity. The depth of cavity is a function of water-layer thickness and number of laser scans. The average depth of cavity of 2 mm depth can be experienced in alumina at 60 W power with 100 scanning cycles and 10 mm/s scan

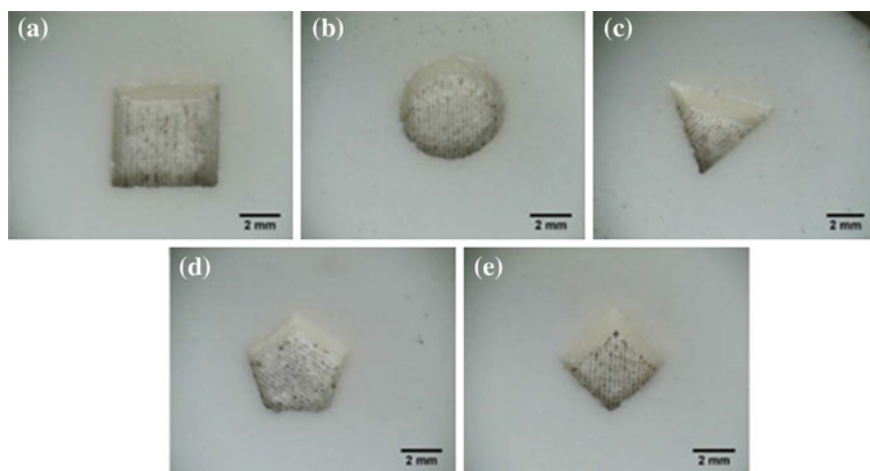


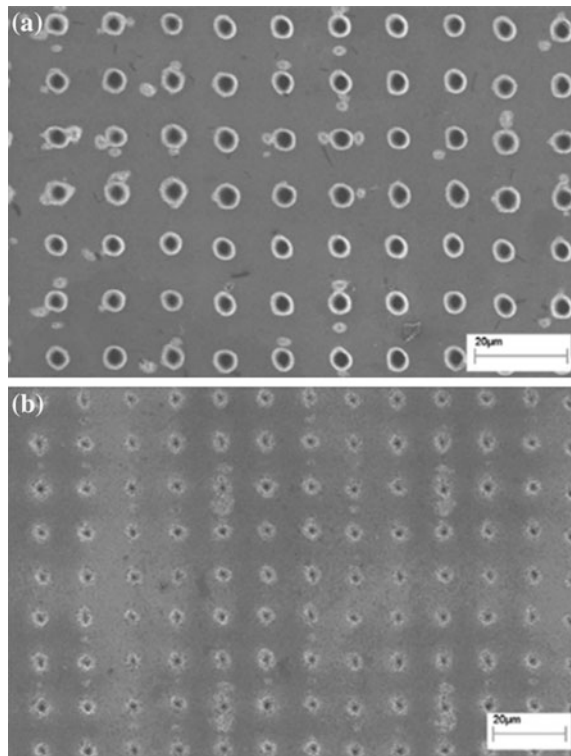
Fig. 17 Optical micrographs of laser underwater machined polygon cavities including **a** square cavity, **b** circular cavity, **c** triangular cavity, **d** pentagon cavity, and **e** prismatic cavity [196]

speed. The kerf width mainly depends on the water layer thickness. Under-water laser milling was found to be expressively competent in terms of surface features especially sidewall and bottom surface appearance compared to machined cavities in air atmosphere. The mechanism study revealed that this was the effect of water dynamics especially the propagation of high recoil pressure that more efficiently ejects the molten material and consequently prevent recast formation and HAZ. In terms of ablated surface appearance of Si, opposite results were presented by [197]. The surface quality of the Si substrate was somewhat rough in case of water than in air. It was figured that the molten silicon rapidly solidified with a dendritic structure. The explanation is justified by the material's specific properties. In order to have more control over the underwater laser ablation process and to eliminate some of the undesired effects in cavity formation and drilling holes, the addition of solvents to the water or machining within a liquid chemical environment could be another option. For example, Voronov et al. [212] used dimethyl sulfoxide as liquid media to process polycarbonate SiC. The ablation rate, however, was low than that in air and water but the surface quality was good.

6.3.3 Under-Water Laser Drilling

Laser drilling in the presence of water is significantly viable compared to dry laser drilling. It is equally suitable for single hole as well as multi-hole arrays with good precision and quality. During the array-hole drilling the first main limitation of dry laser drilling is the hole-distance (greater than 5 mm for brittle materials such as glass and alumina) between the neighboring holes. The second main limitation is the propagation of the micro-cracks and their linkage that ultimately cause the material to be broken or at least unstable. Low aspect ratio is also another drawback of dry laser drilling. All such factual truths can be eliminated/improved by incorporating water environment. The authors of [218] experimentally proved that during the array-hole drilling the hole-distance of even 1–2 mm can be achieved for brittle materials with crack free edges by using 1 mm water layer above work surface. Lu et al. [63] investigated the mechanism behind the quality improvements by underwater laser drilling of various metal plates including copper, aluminum, iron, stainless steel with varying thickness. They concluded that the energy required, to drill a certain hole with constant material characteristics and thickness, is low in case of underwater drilling as compared to dry conditions. Two mechanisms was claimed to appear named as; ablation-produced impact effect and liquid-jet-induced impact effect. The later impact was considered as the main responsible for the high quality drilling results. It has also been proven that the high aspect ratio holes can also easily be achieved by this technique [217]. Kaakkunen et al. [214] investigated the effect of thin film effect in drilling of high aspect ratio (1:13) holes in silicon substrate (Fig. 18). The depth and shape of hole was deeper and uniform in case of spraying water than in air atmosphere. They reasoned it due to the efficient removal of debris by water flow. In the absence of water, the shape of hole become inflicted because of energy scattering by debris. The holes acquired

Fig. 18 The SEM photographs of the ablations made in silicon with (a) and without (b) water spray [214]



curved shape that restricts the subsequent pulses to perform further deep ablation. The detailed mechanism of high aspect ratio etching of UWLA can be found in [213] according to which micro-bubbles generated after laser irradiation develops an upward stream in liquid. That stream with high vapor pressure removes the debris more rapidly. In the study of [198] drilling in SiC has been achieved by UWLA with high precision and quality results than those of drilling in air. The sidewall of drilled hole was found to be free from any visible oxides.

6.3.4 Synthesis of Nano-particles

Nano-materials are of great interest due to their applications in many fields. The structural and efficacy of nano-particles (NP) depend strongly on the method applied for their synthesis. Laser ablation in liquid environment is a simple and effective technique that allows generating mass production of nano-particles from numerous materials (Ag, Au, Ni, Co and Cu-containing solid targets, brass etc.) in the form of a suspension in a given liquid [219]. The liquids could be for example H_2O , H_2O_2 , $\text{C}_2\text{H}_5\text{OH}$, $\text{C}_2\text{H}_4\text{Cl}_2$, etc. This technique retains certain flexibility in controlling the properties of nano-particles by appropriate choice of both laser

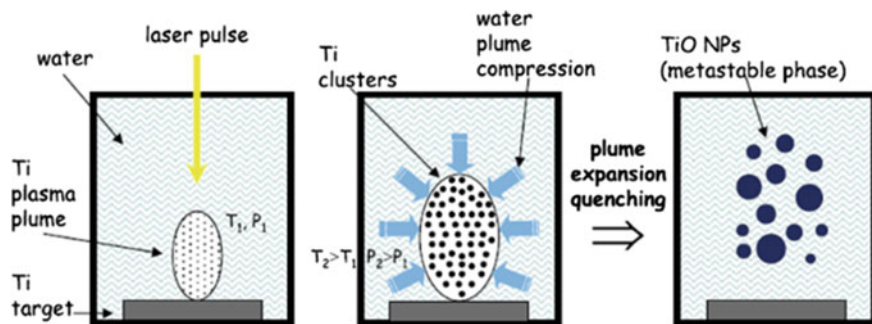
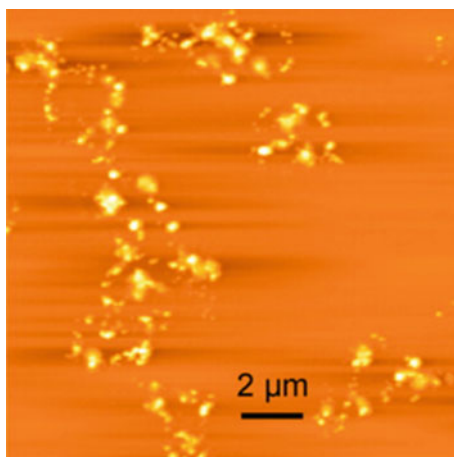


Fig. 19 A schematic diagram of the proposed physical mechanism of formation of TiO NPs in the disordered phase [221]

parameters and the nature of the liquid. Laser ablation in liquid environment is capable of producing NP without any surface active agents or counter-ions, which is indispensable for some applications, e.g. for medical ones [220].

Semaltianos et al. [221] explained the mechanism involved during the fabrication of TiO NPs. Two types of plasma formation were reported namely (1) water plume plasma and (2) ablated species plasma (Fig. 19). The chemical reaction took place between these two plasmas that cause adiabatic expansion and quenching of metastable phases to result in NPs. A sample of NP's produced by pulsed KrF excimer laser is shown in Fig. 20. Zhang and Lan [222] produced nano-particles of nickel (Ni) and cobalt (Co) through laser ablation in organic solution. Pure Ni, Ni50Co50 alloy, and Co metal plates as the targets, respectively, have been irradiated under 532 nm Nd:YAG laser in ethylene glycol. Under the same laser fluence and irradiation time, the average particle size of Ni nano-particles of 8 nm in diameter and 30 nm of Co nano-particles can be achieved. This research

Fig. 20 Atomic force microscopy image of organic NP obtained by underwater laser ablation of PC at 500 mJ/cm², 100 pulses delivered at 1 Hz [224]



demonstrates that laser ablation in liquid, a one-step, non-catalyst process, can produce stable Ni and Co nano-particles. The morphology of NPs mainly depends on the laser fluence. Laser pulse energy has been shown a relatively little effect on the particle size. The investigations of [223] proved that too high pulse energy (e.g. 5 J) could melt the adjacent NPs of aluminum that is useless if the applications require individual NPs. Contrast to this, very less energy (e.g. 1 J) may cause problem of high fragments of aluminum that could not ionized by laser beam. Therefore, they suggested the best energy of 3 J to acquire individual NPs from aluminum under water layer of 5 mm. The boundary level of their energies (1 and 5 J) offered less uniform but smallest size particles (22 nm and 27 nm respectively). While the optimum level of energy (i.e. 3 J) offer more uniform, spherically shaped particles but with largest size (48–100 nm).

Mahfouz et al. [225] explained the ablation of Ni targets in water by laser impact (532 nm, 40 mJ/pulse, 10 Hz and 8 ns duration) focused on massive samples (~ 2 mm diameter) that generate colloids with fine nano-particles. The amount of metal released in the solution increases first linearly with time, but slows down after 8 min of impact. This decrease the ablation efficiency. The reason behind could be the related to the abundance of nano-particles. The interaction rate of NPs with the incoming laser beam become high that that could lower the laser power on metal surface or modify the surface properties which diminish the ablation efficiency. The size distribution of the nano-particles thus produced can be in the range 3–5.3 nm in diameter, with a tendency for the size to be smaller for larger number of laser shots. Because of nickel and oxygen reaction, in fact, nickel oxide nano-particles are produced, rather than nickel nano-particles. Gondal et al. [226] applied pulsed laser ablation (PLA) technique in 3% H_2O_2 aqueous solution to synthesize nano-sized nickel oxide (NiO) particles. This work demonstrates that PLA is an effective method to control the size, impurity and minimal chemical waste generation which is the major problem with other wet chemical methods. Huang et al. [227] synthesized titanium nano-particles and nanotubes from pure titanium under PLA processing in the presence of water. Compagnini et al. [228] worked on the formation of Molybdenum disulfide (MoS_2) fullerene-like nano-particles by the laser ablation of crystalline targets in water and found that NP of size 10–15 nm diameter can easily be obtained in single step.

Laser fluence have the direct influence on the morphology of NPs. However, irrespective to the laser parameters, the shape and composition of NPs also depends on the nature of the liquid used [220]. For example, laser ablation of titanium immersed in ethanol results cubic structured particles. The immersion of titanium in dichlorethane after laser irradiations build TiC particles instead of solely titanium particles. Finally, the water immersion allows to produce TiO NPs having the composition of non-stoichiometric oxides. Among these fluids the size of NPs found to be smallest in case of water [229]. In general terms, the aqueous environments have the ability to alter the chemical composition of NPs compared to the bulk material due to the high chemical reactivity of water at elevated temperature gained during ablation. For instance, the ablation of Cu immersed in water produce Cu^+ ionic states instead of pure Cu particles [230]. Modifications in chemical

composition can also be found for ablation of Si. The water immersion produce amorphous SiO_2 while ablation in ethanol results in the formation of Si nano-particles having an outside shell of oxide. This oxide shell can also be observed in some other metals as well. However, there are certain materials which don't react with the surrounding environments and retain their stoichiometry after laser ablation. This concern, for example, NPs of CdS or CdSe obtained via laser ablation of semiconductor under water, acetone and other liquids. NPs of CdS showed a strong crystallinity while processing in different liquids. Similarly, ZnSe fabricated through laser ablation under different liquid environments revealed almost perfect stoichiometry [231].

6.4 Conclusions and Remarks

The inspirations of UWLA on ablation performance are undeniable. This confining process looks favorable for various real-world applications in surface treatment aided by laser. The following list of conclusion can be drawn from this section:

1. This hybrid process has the potential to significantly control the core drawbacks of dry laser ablation.
2. In terms of ablation rate mix of results are published by numerous researchers.
 - (a) Most of the research outcomes favor the high ablation in the presence of water compared to dry laser ablation.
 - (b) There are many authors who claimed low ablation rate by UWLA in comparison with air atmosphere.
 - (c) The common reason behind this conflict is stated as the particular behavior of the target material or the specific experimental conditions.
3. The work position relative to laser beam contributes significant role in the ablation mechanism, material ejection and ablation rate. The configuration of vertically oriented work target and horizontally oriented laser beam gives improved results.
4. Water layer thickness above specimen surface is one of the key parameter in UWLA. In general, 1–4 mm layer thickness is demonstrated to achieve high MRR.
5. With respect to UWLA machining characteristics drilling, milling and crater formation have been found the main research themes resulting in good surface morphologies and less thermal damage as compare to laser ablation in air atmosphere.
6. In another highly positive aspect the process is greatly promising and simple to achieve nano-particles from a wide range of materials under different liquid environments. Although, most of the NPs are not pure as the bulk target material. The chemical composition of the particles changes depending upon the environment and compel to propagate some carbides and oxides.

7 Micro-channels Applications and Fabrication

Microchannel heat exchangers have applications in several important and diverse fields including: aerospace; automotive; bioengineering; cooling of gas turbine blades, power and process industries; refrigeration and air conditioning; infrared detectors and powerful laser mirrors and superconductors; microelectronics; and thermal control of film deposition. The advantages of microchannel heat exchangers include high volumetric heat flux, compactness for space-critical applications, robust design, effective flow distribution, and modest pressure drops. This section will cover selected industrial examples for microchannel heat exchangers, microchannel heat pipes, and microchannel heat plates [16].

7.1 Micro-channel Heat Exchangers

7.1.1 Automotive and Aerospace

Microchannel heat exchangers have at least one fluid flow passage with typical dimensions between 10 and 1000 μm and have great potential in process intensification of various industrial areas [232]. There are many possible channel geometries for microchannel heat exchangers, two types of which are the most widely used in compact heat exchanger designs for automotive and aerospace applications. These are shown in Figs. 21 and 22. High-temperature and compact micro heat exchangers can be manufactured using ceramic tape technology [233],

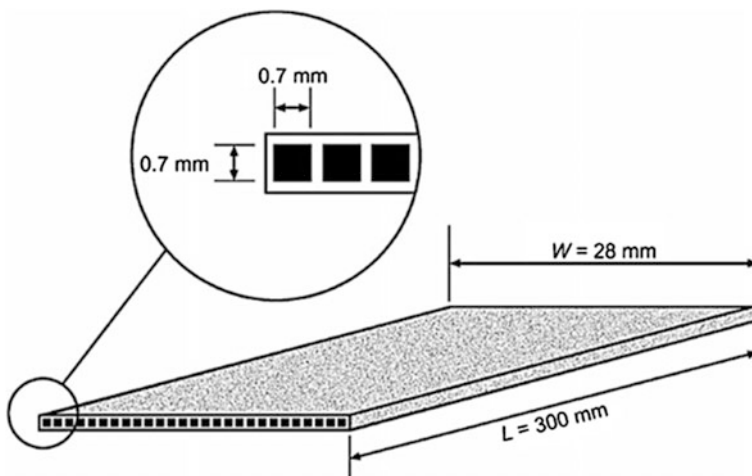


Fig. 21 Typical dimensions of a rectangular microchannel for compact heat exchanger applications [16]

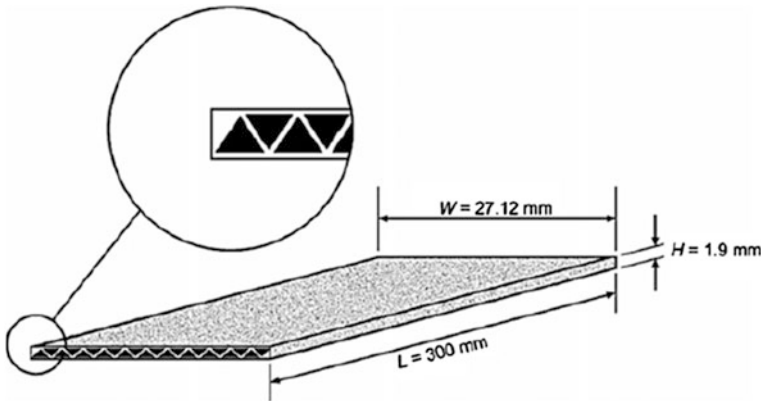


Fig. 22 Typical dimensions of a triangular microchannel for compact heat exchanger applications [16]

which uses fused ceramic layers to create channels with dimensions below 1 mm [233]. Metal-based microchannel heat exchangers are also of current interest because of the combination of high heat transfer performance and improved mechanical integrity [234]. Figure 23 shows a manufactured, flat extruded multi-channel aluminum heat exchanger.

In recent years major progress in microchannel heat exchangers has been made by the automotive, aerospace, chemical reactor, and cryogenic industries. Thermal duty and energy efficiency requirements have increased during this period, while space constraints have become more restrictive. The trend has been toward greater heat transfer rates per unit volume. The hot side of the evaporators in these applications is generally air, gas, or a condensing vapor. With advances in the airside fin geometry, heat transfer coefficients have increased, as have surface area densities. As the air-side heat transfer resistance has decreased, more aggressive heat transfer designs have been sought on the evaporating side, resulting in the use

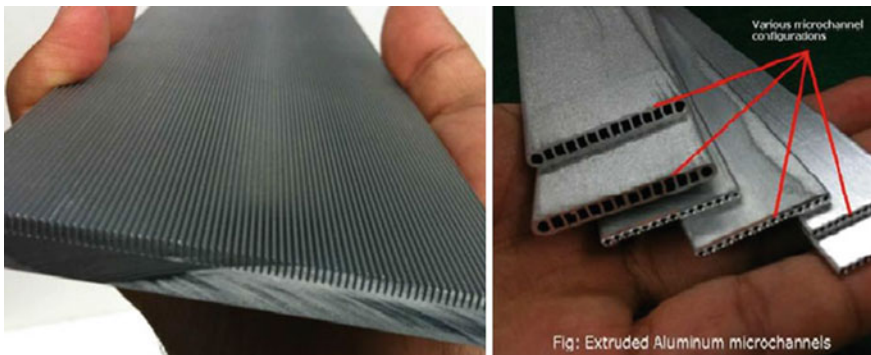


Fig. 23 View of a microchannel heat exchanger [16]

of microchannel flow passages on the liquid side (evaporating or condensing or single-phase regimes). The major changes in recent evaporator and condenser designs for automotive and other compact heat exchanger applications involve the use of individual, small-hydraulic-diameter flow passages arranged in a multi-channel configuration on the liquid side. The ability to efficiently transfer heat between fluids using lightweight, compact heat exchangers is important in a variety of applications, such as automobile radiators, air conditioning, and aerospace applications. Microchannel heat exchangers are well suited to these applications due to the micro-channels' compactness, lightness, and high heat transfer performance.

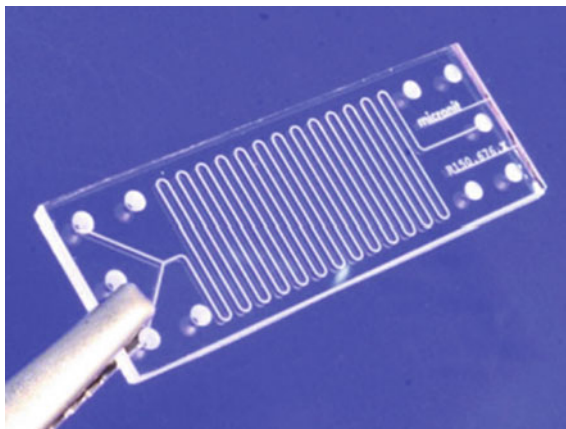
Car radiators employ a cross flow design that allows a sufficient mass flow rate of air through the radiator while using only the stagnation pressure associated with the motion of the automobile. The common measure of performance for car radiators is the heat transfer/frontal area normalized by the difference in inlet temperatures of the coolant (water–glycol) and the air. For conventional car radiators, 0.31 W/Kcm^2 of heat transfer/frontal area can be obtained between the air and the coolant. The cross flow microchannel heat exchanger can transfer more heat/volume or mass than existing conventional heat exchangers within the design constraints. This can be important in a wide range of applications (automotive, home heating, and aerospace).

A review by Sommers et al. [235] discussed numerous applications that particularly benefit from ceramic heat exchangers. Ceramic materials offer potentially significant advantages compared to metal alternatives, including significantly higher operating temperatures, improved tolerance of harsh chemical environments, improved bonding with ceramic-based catalyst and significant cost savings in materials and manufacturing methods. Although there are numerous possible applications, the effort reported here is motivated by the need for low-cost, high-performance fuel reformers, and the need to effectively integrate unit processes in solid-oxide fuel cell systems. The microchannel reactor integrates the upstream fuel heating and reforming with downstream recuperation to harness the high-quality heat exiting the tail-gas combustor. Such process intensification can improve system efficiency. It is feasible to further combine processes by catalytically activating both sides of the microchannel reactor, using one set of layers for upstream fuel reforming and the opposite set for tail-gas combustion.

7.1.2 Chemical Reactors

Microchannel chemical processing technology is an emerging field with applications in most industrial processes due to its excellent mixing capabilities, controlled reaction environment, and energy efficiency. This technology offers improvements in existing processes and will enable new processes to become cost effective. The basic microchannel reactor design is based on the flow between parallel platelets coated with a catalyst. The large aspect ratio of the channel provides extensive surface area in a small volume. Microchannel reactors have been developed based

Fig. 24 Glass micro-reactor: the channels of the chip in the picture are $150\ \mu\text{m}$ wide and $150\ \mu\text{m}$ deep [16]



on ceramic substrates as well as metal substrates. In both types of reactors, multiple layers coated with catalytic material are bonded, forming a monolithic structure. An added benefit of a layered pattern is the ability to easily scale up or down by adjusting the number of layers. This provides great flexibility in the design, since if the production capacity needs to be changed, there is no need to redesign the reactor. Figure 24 shows a manufactured micro-reactor.

Falling-film Micro-reactors

Falling-film micro-reactors work in the same way as macro-scale absorbers. Microchannel falling-film absorbers have been reported in the open literature by [236–238]. The central part of the micro-reactor is a stainless steel plate containing 64 vertically positioned micro-channels ($300\ \mu\text{m}$ wide and $100\ \mu\text{m}$ deep). Liquid spreads to form a thin film among the micro-channels and flows further downward to the withdrawal zone at the bottom. Gas flows in a large gas chamber positioned above the microchannel section, facilitating concurrent or countercurrent operation mode. Figure 25 shows a schematic of a falling-film and microbubble reactor.

Membrane Separation Technology

In membrane separation technology, gas and liquid flow in two different channels, separated by some physical structure, such as a mesh, selective membrane, or micro-porous plate [239]. Oak Ridge National Laboratory and Velocys Inc. separated liquid and vapor phases in micro-channels by membrane in a traditional counter-flow arrangement. The membrane prevents the liquid from bridging the microchannel and maintains stable phase separation. However, it significantly decreases the surface area of the liquid–gas interface. Figure 26 shows the opening area of the membrane comprising just about 10% of total surface area.

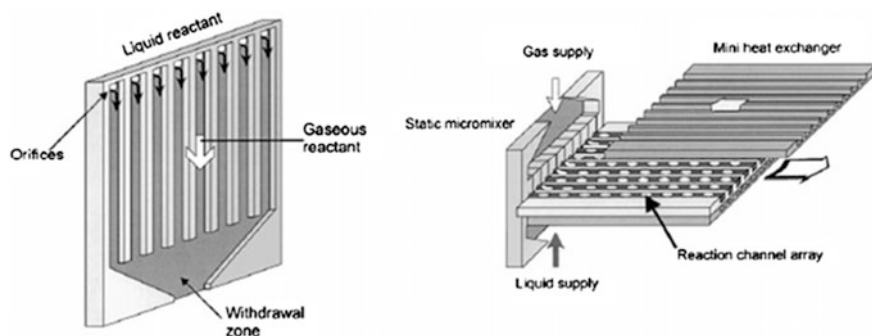


Fig. 25 Falling film and microbubble reactors [238]

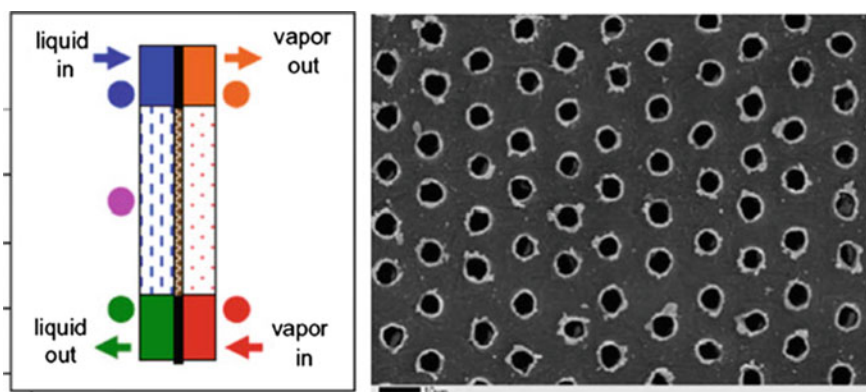


Fig. 26 Counter-flow absorber and phase separating membrane (Velosys Inc.)

Co-current Micro-channel Absorption

In the co-current configuration, gas, and liquid flow concurrently in the same microchannel, creating various types of flow patterns similar to that of two-phase flow in a tube. The liquid film is maintained by shear stress of the moving gas phase, and film thickness can be ultimately small. Channel hydraulic diameter can be significantly smaller, limited only by the desired fouling characteristics. With co-current flow, films of a few microns thick can be arranged on the channel wall, and associated with this thickness very high mass transfer coefficients can be obtained [240]. Figure 27 shows a schematic of the concurrent microchannel absorption process.

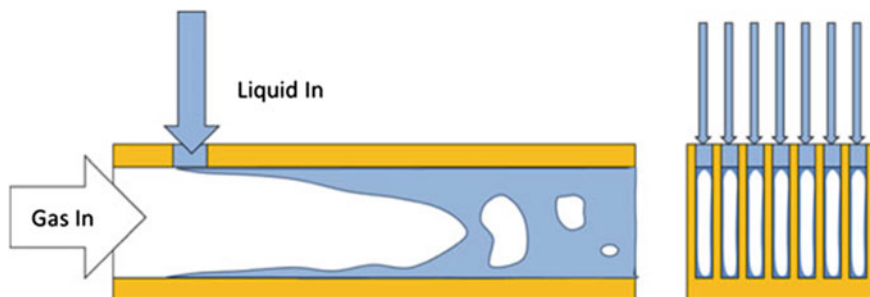


Fig. 27 Co-current micro-channel absorption process [240]

7.1.3 Cryogenic Systems

Microchannel heat exchangers are used in cryosurgical probes for ablating tumors or treating heart arrhythmia [241], as shown in Fig. 28a. The Joule–Thomson cryocooler is most widely used for the cryosurgical probe. The advantages of the Joule–Thomson cryocooler include its simple structure and compactness and the lack of electrical interference. The heat exchanger of the subminiature Joule–Thomson refrigerator used in the cryosurgical probe has channel diameters from tens of microns to hundreds of microns, according to space limitations. Figure 28b, c show schematic diagrams of a cryosurgical probe and a cryosurgical system for use in cancer surgery. In many cryogenic applications, the desired heat transfer, which is

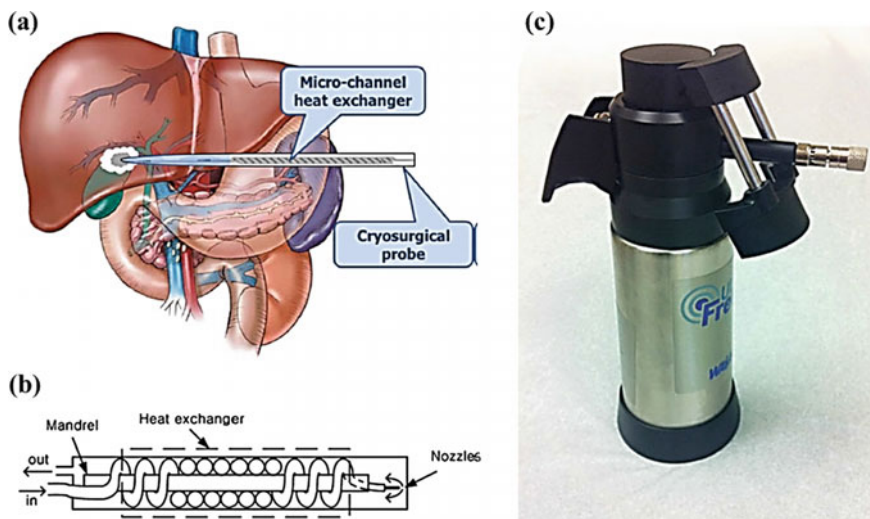


Fig. 28 Micro-channels in cryosurgery; **a** treatment of a cancer by cryosurgery, **b** schematic diagram of a cryosurgical probe and **c** cryosurgical system for surgery of cancer [241]

the refrigeration load, is a small fraction of the heat transferred within the heat exchanger. In this case, the ineffectiveness of the heat exchanger must be an even smaller number, and the effect of axial heat conduction and parasitic heat transfer can dominate the performance of the device. Furthermore, the large absolute temperature change within the heat exchanger produces correspondingly large variations in the properties of the fluids and metal that can also affect performance.

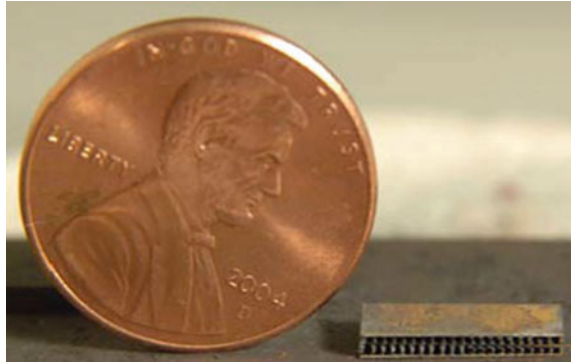
7.2 *Laser Diode Applications*

Microchannel cooling is now a mature technology, over 30 years old and widely used on a commercial basis in the high-power laser diode industry. Microchannel coolers are also now being used in commercial systems to cool LEDs in UV curing systems and photovoltaic cells in concentrated solar power systems. The present commercial cooling technologies, however, will not be adequate as power levels of semiconductor devices increase. Since laser diodes have stringent performance requirements and are by far the largest commercial market share of microchannel coolers, the remainder of this discussion will focus on laser diode applications. Commercial coolers generally employ water-cooled copper micro-channels to dissipate up to 1 kW/cm^2 from semiconductor heat sources ranging from 0.1 to 2 cm^2 in size. These coolers use rectangular ducts with widths from 25 to $200 \text{ }\mu\text{m}$, duct aspect ratios up to $15X$, and flow rates ranging from 10 to $30 \text{ gm/cm}^2/\text{W}$ (based on heated area). These parameters result in thermal resistances of $30\text{--}75 \text{ K-cm}^2/\text{kW}$, with pressure losses between 10 and 50 psi . There are four main ways future commercial microchannel systems can be improved: (1) reducing the cooler thermal resistance; (2) reducing package thermal resistance through use of reduced thermal expansion coolers; (3) reducing flow rate to minimize system costs of cooling; and (4) increasing operating lifetime. Reducing channel width is promising: for water-cooled systems, reducing the channel width of a copper microchannel cooler to $\sim 12.5 \text{ }\mu\text{m}$ results in thermal resistances in the $15\text{--}20 \text{ K-cm}^2/\text{kW}$ range with reasonable pressure losses. Secondary features can offer performance improvements for larger channels (channel width $> 100 \text{ }\mu\text{m}$), but they cannot be economically fabricated in smaller channels. Diamond is well known for its outstanding thermal conductivity, but it is difficult to machine with micro-passages. Figure 29 shows a prototype diamond microchannel cooler fabricated by laser etching thin ($100 \text{ }\mu\text{m}$ thick) diamond sheets and brazing the sheets together. This approach was not able to create passages narrower than $250 \text{ }\mu\text{m}$ [242].

7.3 *Micro-channel Heat Pipes*

Because advanced electronic equipment is decreasing in size, the circuit integration per unit area must increase, which in turn contributes to a rapid increase of heat

Fig. 29 CVD diamond microchannel cooler with $250 \times 300 \mu\text{m}$ rectangular ducts [242]



generation rates. As a consequence, the operating temperatures of electronic components may exceed the desired temperature level, and if heat is not sufficiently removed, the failure rate of the equipment will cause an accelerated system failure. Due to the compactness of most modern electronic components, cooling devices also need to be small but highly effective in heat transport. Wicked heat pipes (or capillary-force-driven heat pipes) evaporate and condense the working. Recently, microchannel technology has been applied to the fabrication of micro heat pipes. Many experiments have been conducted on microchannel heat pipes. Cotter [243] first introduced the concept of a micro heat pipe that did not include a complicated wick structure. Kang and Huang [244] and Berre et al. [245] have studied silicon micro heat pipes with a polygonal cross-section. The silicon micro heat pipes use the sharp edges of the polygonal groove for return of the condensate to the evaporator. Although silicon micro heat pipes are small and can overcome the thickness limitations of wicked heat pipes, they cannot handle a large amount of heat, and their performance has yet to be improved.

7.4 *Micro-pulsating Heat Pipes*

Youn and Kim [246] developed a micro-pulsating heat pipe that did not have a wick structure and instead contained rectangular micro-channels forming a meandering closed loop. The heat was transferred from an evaporator to a condenser by means of the axial oscillation of liquid slugs and vapor slugs. This micro-pulsating heat pipe has progressed beyond research laboratories and is now under mass production. As shown in Fig. 30, micro-pulsating heat pipes with looped micro-channels were fabricated by MEMS or micro-machining technology. The fabrication of the micro-pulsating heat pipe was completed by bonding the top cover plate and filling the pipe with a working fluid. Then the heat input and output were connected at the evaporation and the condensation sections, respectively. A total of 10 parallel, interconnected rectangular channels forming a meandering closed loop were

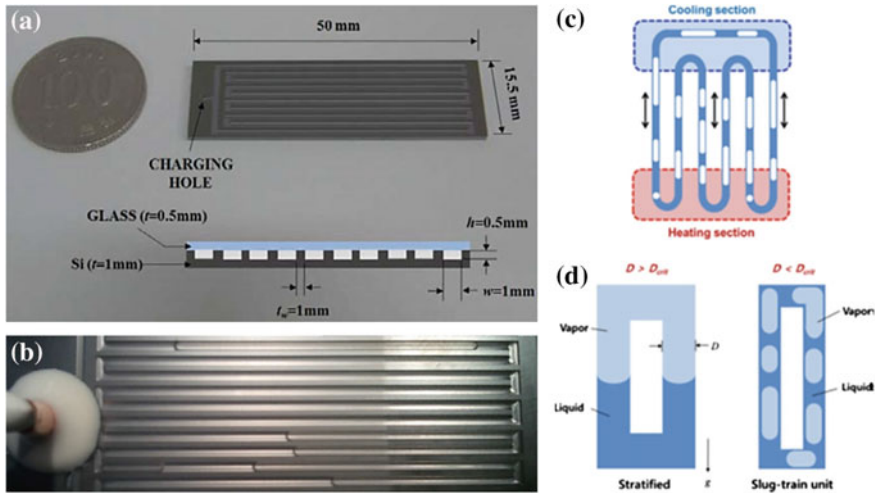


Fig. 30 Micro-pulsating heat pipe; **a** CAD model with dimensions and **b** top view of the micro-pulsating heat pipe with filling ratio of 50%, **c** working principle of micro-pulsating heat pipe, **d** vapor and liquid arrangement according to tube diameter [246]

engraved on the silicon wafer with a thickness of 1 mm. The top of the silicon wafer was covered by a transparent glass plate with a thickness of 0.5 mm to allow visualization of the internal thermos-hydrodynamic behavior in the micro-pulsating heat pipes. The silicon wafer and glass plate were bonded together using anodic bonding. A hole of 1 mm diameter was drilled on the top of the glass plate to evacuate the micro-pulsating heat pipes and fill the micro-pulsating heat pipes with working fluid. Figure 30 represents the fabricated micro-pulsating heat pipes and dimensions of the heat pipe. The overall micro-pulsating heat pipes had a length of 50 mm, width of 15.5 mm, and thickness of 1.5 mm. The width and height of the engraved rectangular channel were 1 and 0.6 mm, respectively, and the hydraulic diameter was 0.75 mm. Ethanol was used as a working fluid. The micro-pulsating heat pipes achieved maximum effective thermal conductivity of 600 W/m K and a maximum heat transport capability of 4 W.

The heat is transported from the evaporator to the condenser by means of local axial oscillations and phase changes in the working fluids. A manufactured micro-pulsating heat pipe is shown in Fig. 30b, in which the boundary between the liquid slugs and the vapor slugs is distinguishable. The micro-pulsating heat pipe has many advantages, including high thermal performance and a maximum effective thermal conductivity of about 600 W/m_K, which is 3.5 times higher than that of silicon ($k = 162$ W/m_K) and 1.5 times that of copper ($k = 400$ W/m_K). It is possible to make a small, thin, and flat structure, and if a flexible material is used for the base and cover materials, it is possible to make a flexible micro-pulsating heat pipe because there is no wick structure.

As shown in Fig. 30c, the heat was transferred from the evaporator to the condenser sections by means of the axial oscillation of liquid slugs and vapor slugs.

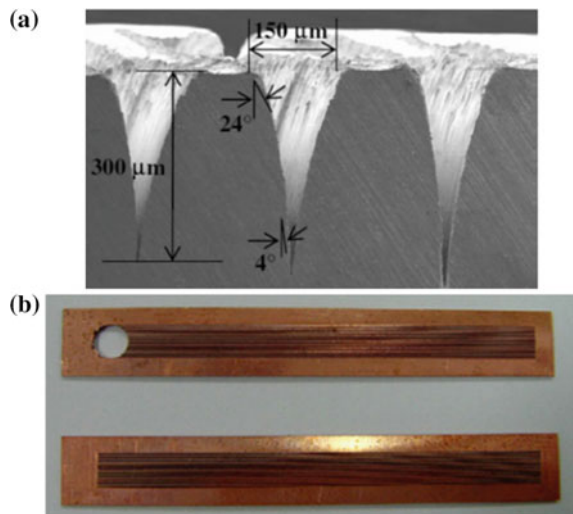
The micro-pulsating heat pipe is different from conventional heat pipes in design and working principle. There is no wick structure to return the condensed working fluid back to the evaporator section. The micro-pulsating heat pipe is made from a long meandering continuous capillary tube bent into many turns. The diameter of the tube is made sufficiently small that vapor plugs can be formed by capillary action as shown in Fig. 30d.

7.5 Micro-channel Flat Heat Pipes

The potential devices for which the flat micro heat pipes fabricated may be applied are mobile electronics such as small notebook PCs, PDAs, or cellular phones. Although conventional heat pipes use either wire mesh or sintered metal for the wick structure that is attached to the inner surface of a sealed metal housing, it is difficult to adopt the same approach in micro flat heat pipes, as MHP size cannot be reduced below a certain limit, for instance of 2–3 mm in thickness, due to the volume of the wick structure itself. Thus, the flat micro flat heat pipes should occupy as little space as possible to fit in the already small mobile device. Also, since the main heat source in an electronic device is a chip, and the sides of most chips are flat, the flat micro flat heat pipes are designed in a flat rectangular shape with a thickness of 1.5 mm. Recently, Lim et al. [247] developed a micro heat pipe with a microchannel groove wick structure using laser micro-machining technology. The structure of the microchannel grooves of a micro flat heat pipe is shown in Fig. 31a.

A manufactured micro-pulsating heat pipe is shown in Fig. 31b. The working principle of the micro flat heat pipe is the same as that of a conventional heat pipe with a porous wick structure. The heat is transferred from an evaporator to a

Fig. 31 Micro-channel flat heat pipe; **a** structure of microchannel grooves and **b** top view of the micro flat heat pipe [247]



condenser. When one end of the heat pipe is heated, the working fluid inside the pipe at that end evaporates and increases the vapor pressure inside the cavity of the heat pipe. The latent heat of evaporation absorbed by the vaporization of the working fluid reduces the temperature at the hot end of the heat pipe. The heated vapor moves to the condensation section and condenses back into a liquid at the cold interface, releasing the latent heat. The liquid then returns to the hot interface through the capillary action of the microchannel grooves, where it evaporates once more and repeats the cycle. The micro flat heat pipe has many advantages, including its small, thin, and flat structure. It also has high thermal performance, with a maximum heat transfer rate of 8 W under stable operation and 13 W at the dryout point.

7.6 *Micro-channel Heat Plates*

A micro-channel plate (MCP) is a planar component used to detect particles (electrons or ions) and impinging radiation (ultraviolet radiation and X-rays). A typical MCP consists of about 10,000,000 closely packed channels of common diameter, formed by drawing, etching, or firing in hydrogen, forming a lead glass matrix. Typically, the diameter of each channel is 10 μm . Each channel acts as an independent, continuous dynode photomultiplier. MCPs are widely used to intensify low-light signal inside various image detectors. Industries for MCP applications range from astronomy to aerospace, machine-building, experimental physics, chemistry, biology, medicine, and ecology.

7.7 *Micro-channel Fabrication Techniques, Materials, Sizes and Shapes*

7.7.1 *Fabrication Techniques*

There are many techniques to produce above said sizes and shapes of micro-channels including both the conventional as well as non-conventional techniques. But every manufacturing process has its own limitations. For example, the conventional micro-milling process using micro-tools are commonly used but the high tooling cost, burr formation, material constraints offered by difficult-to-machine materials, chip adhesion, high thrust forces, heat affected zone and striation marks are the obvious drawbacks of conventional micro-milling and consequently restrict the process for precise micro-featuring especially in hard-to-machine materials such as titanium and nickel alloys [32–36]. Fabrication of micro-channels in Ti-6Al-4V has been realized by Vazquez et al. [37] with the help of tungsten carbide micro-tools using CNC machining center. Micro-hot embossing is another potential candidate among the available technique of micro-channel

production. The process of micro-hot embossing was utilized by the researchers of [22] while manufacturing an array of micro-channels of size 5–100 μm in aluminum target material. Gau et al. [38] proposed a flexible die forming process to form micro channels in aluminum foils (foil thickness 50 and 75 μm). They produced micro-channels of width size less than 1000 μm . Vacuum die-casting is another cost effective method if the objective is to produce array of micro-channels on large areas such as required in components used in proton exchange membrane fuel cells. Jin and Kang [23] fabricated such arrays of micro-channels on both sides of bipolar plates of aluminum alloys by vacuum die-casting. Among non-traditional machining process electric discharge machining (EDM) is considered as relatively good alternative having no material hardness and channel shape restrictions [13, 24]. But there are also number of problems linked with EDM and wire-EDM such as low productivity, high tool wear rate, lack of precision due to tool wear, unsuitable for batch production or multi-channels [39], thick recast layer (from 2.5 to 30 μm) [40], heat affected layer of 40–100 μm [40], thick white layers (6–8 μm) with micro-cracks [41], poor surface integrity [42] and necessary post processing requirements [43]. Chemical etching is another alternative for the fabrication of micro-channels but it offers troubles of having high aspect-ratio micro-channels [44]. The comparison of different machining methods in terms of advantages and shortfalls is shown in Table 4.

Laser beam micro-milling (LBMM) is considered as among the competent techniques used for micro-fabrications. It is well suited for machining of a wide range of materials; from ductile to hard-to-machine materials. LBMM using Nd:YVO₄ nano-second laser can be found to produce circular cross-sectional micro-channels on soda lime glass [45]. Similarly, femtosecond laser has been utilized by a research team of [46] where they generated micro-features on different polymeric samples. Selection of channel size is also important and should be considered alongside the laser parameters. Wider sized channels with relatively good dimensional accuracy can be more flexibly produced in titanium alloy by Nd:YAG pulsed laser compared to the accuracy in narrow sized [47]. Likewise, the processing of metals (aluminum and titanium) by laser milling has been documented in [48] where width and depth of micro-features were studied. Aluminum and steel based alloys dealt under nano-second pulsed fiber laser are presented in [49] where the authors examined the effect of laser based parameters on the formation of micro-notches. As per their conclusions the micro-notches vary in sizes and the machined width and depth mainly depend on laser power and pulse repetition rate. Another study stated that laser milling is a complex process due to which a variation in depth and width of micro-channel can be soundly observed [50]. They applied Nd:YAG laser to machine micro-channels of size 200 \times 50 μm . In general, for polymeric materials, the micro-channel's geometry (width and depth) primarily relies on laser power and scanning speed under linear relationship. However, the frequency of laser pulses does not severely affects the channel's depth and width [51]. The microchannel grooves can be fabricated by laser micro-machining, MEMS, or LIGA technologies. The microgrooves of the micro flat heat pipe were fabricated on copper foil using a femtosecond laser

Table 4 Different machining processes; advantages and shortfalls

Process/operation	Geometry/tools	Advantages	Shortfalls	References
conventional drilling	Holes through modified twist drills Holes by gun-drilling	High aspect ratio 50% increase in tool life by Coating	Drill damage High wear High heat generation Tool degradation Poor Straightness Burs at edges High tool cost	[248, 249]
Conventional milling	Diamond-like coated micro-end mill (\varnothing 760 μ m) WC-Co micro milling tools Micro-grooves by Diamond tool	High material removal rate (3401 mm ³ /min) [32] Smaller cutting forces Better surface finish	High cost of micro-tools Chip adhesion High thrust forces Heat affected zone Striations	[32–36]
Conventional turning	Coated tools Uncoated tools	Improves hardness Work hardening layer (around 100 μ m)	Surface tearing Cavities, Cracking Metallurgical recrystallization Plastic deformation Residual stresses	[250–253]
EDM/WEDM (cutting, milling and drilling)	Fir tree slots by brass wire, Coated high speed cutting wire [254] Flat bottomed tool [255] Powder Metallurgy Processed CuW Electrode [256]	Material removal efficiency in W-EDM [41] Reduced machining stresses Improved micro-hardness (from 380.9 to 496.7 HV) [256] Lesser metallurgical damage Complex features Less heat affected layer	Low productivity (0.47 \times 10 ⁻⁸ mm ³ /min) Tool wear rate (5.6 \times 10 ⁻⁹ mm ³ /min) Suitable for small batch size [39] Lack of precision due to tool wear Poor cylindricity Thick recast layer (from 2.5 μ m to 30 μ m) [40] Heat affected layer 40–100 μ m [40] Thick white layers (6–8 μ m) with micro-cracks [41]	[39–43, 254–260]

(continued)

Table 4 (continued)

Process/operation	Geometry/tools	Advantages	Shortfalls	References
ECM		High material removal rates Good surface integrity [261] Less heat affected zone [262]	Micro-cracks [257, 258] Poor surface integrity [42] Post processing requirements [43] Less fatigue life [259] High tooling cost Suitable for large batch sizes [39] Salt film on machined surface [261] Selective corrosion due to the formation of a porous salt film [263] Current density ($<5 \text{ A cm}^{-2}$) results undesirable dissolution [263]	[39, 261–265]
Air/abrasive/water jet (cutting and milling)	3D pockets ($20 \times 20 \text{ mm}$) [264]	No tool required Very less thermal effects	Surface striations Waviness [265] Surface waviness ($W_a = 7.53\text{--}10.37 \mu\text{m}$ for NiTi shape memory alloy) [266] Undercut to the designed geometry [264] Surface roughness ($R_a = 2\text{--}8 \mu\text{m}$ for Inconel) [267] surface residual stress Compressive stresses [268, 269]	[266–269]
Ultrasonic/vibration assisted (cutting, turning, milling, drilling and grinding)		Improve surface roughness by 9.10–51.61% Decrease cutting force by 32.34–24.47% [270] Improve drill life [271] Decrease working time [271] Reductions in vertical and horizontal forces [272]	large vibration amplitudes lowers drill life [271] Greater wheel wear (30–60%) Increase roughness (up to 24%) [272] Overlapping grit marks [272]	[270–274]

(continued)

Table 4 (continued)

Process/operation	Geometry/tools	Advantages	Shortfalls	References
Laser/plasma assisted (cutting, drilling and surface modification)		Less stresses in the tools [273] 30% reduction in cutting force [150] Improved surface roughness 40% [275, 151] Increase in tool life [275, 276] No micro-crack during laser surface melting [277] Increase in Hardness by laser surface treatment [278]	Compressive residual stresses [151] Thicker compressive zone (40–70 µm) [279] Hardness reduction [276] Heat affected zone [280] Striation formation Micro-cracking Oxide layers [281] Kerf taper Recast layer [282] Residual stresses [278]	[150, 151, 153, 275–282]

micromachining technique. A commercial chirped pulse amplification laser system and a translation XYZ stage were used to fabricate the grooves under normal atmospheric air. The laser beam was focused on the workpiece using a $10\times$ objective lens, and the workpiece was firmly attached on the translation stage using tape. The microgrooves, which serve to facilitate liquid passage during operation, were machined on the top and bottom plates. The width, depth, and length of each microgroove were about 150, 300, and 50 mm, respectively, and 16 grooves were produced on each plate.

7.7.2 Micro-channel Materials

Several materials on which the micro-channel fabrication is required are used in different kinds of applications. The choice of material depends on the requirements and systems where the micro-channels have to serve for cooling applications. For example, copper micro-channels are used for heat sinks cooling [13] and silicon micro-channels for particle physics detectors [11, 21]. Micro-channels in aluminum alloy can be found in [22–24]. Very less study is done on fabrication of micro-channels in hard-to-machine materials like titanium and nickel alloys. The fabrication of micro-channels in non-metallic can be found in various studies showing micro-channels produced in Polycarbonate (PC) [25], poly-methyl methacrylate (PMMA) [26], Polydimethylsiloxane (PDMS) [27] and boro-alumino-silicate glass [28].

7.7.3 Micro-channel Shapes and Sizes

In terms of micro-channel's cross-sectional shapes, different shapes are reported in literature including rectangular [29], triangular [21], trapezoidal [30] and circular cross-section micro-channels [31]. In one of the study, a unique Ω -shaped cross section was seen where the researchers study the effect of micro-channel shape on flow boiling performance of fluids passing through micro-passages of the channels [13]. They also compared the performance of Ω -shaped micro-channels with rectangular shaped micro-channels. The most common type of micro-channel cross section found in literature is the open ended v-shaped or u-shaped square/rectangular cross section. The shape and size of micro-channel directly influence the fluid flow characteristics, heat transfer process, pressure drop characteristics and two-phase flow instabilities. For example, 100 parallel micro-channels having equal sizes of $100 \times 680 \mu\text{m}$ have been fabricated in multichannel heat sink used for cooling of micro-electronic central processing unit to study the two-phase flow boiling of R134a refrigerant [12]. In another similar study, the air and water (two-phase) flow performance is studied in hybrid micro-channel solar cell by fabricating an array of rectangular micro-channels with a hydraulic diameter of $667 \mu\text{m}$. To meet a similar objective, the authors of [29] used three high-aspect-ratio rectangular shaped micro-channels having the hydraulic diameters of 571, 762 and $1454 \mu\text{m}$.

7.8 *Conclusions and Remarks*

Micro-channels have proven tremendous applications in several engineering and biomedical fields. From the brief literature reviewed with respect to the micro-channels applications and fabrication techniques, following conclusions may possibly be drawn:

1. The micro-channels are extensively used in various fields including engineering, aerospace, automotive, and biomedical applications. The micro-channels are utilized in the form of micro-heat exchangers, micro-reactors, micro-channel heat plates, and micro-pulsating heat pipes etc.
2. Fluid flow dynamics inside the micro-channels plays an important role to design the precise process where the micro-channels are required. The flow boiling performance of fluids passing through micro-passages of the micro-channels is widely attempted. About the fluid flow dynamics, a common inference can be established that the flow boiling performance inside the micro-channels depends on the shape and size of micro-channels.
3. There are several techniques to produce micro-channels on different materials, such as micro-CNC machining, micro-hot embossing, micro-forming, micro-die casting, chemical etching, electric discharge machining (EDM) and laser beam machining (LBM). Among these techniques, laser beam machining is considered as the most flexible micro-channel fabrication process in terms of flexibility in material and production, quality, size, and shape.
4. Depending on the application requirements, almost all kinds of materials including metals and non-metals are used for the fabrication of micro-channels of several sizes. Selection of micro-channel size solely depends on the fluid flow requirements. That is why, a number of micro-channel sizes can be found in several researches and thus, the literature is dense in this regard. In terms of micro-channel's cross-sectional shapes, different shapes are reported in literature including rectangular, triangular, trapezoidal and circular cross-section micro-channels. However, the rectangular shaped micro-channels are most widely attempted and required.

8 *Literature Review Conclusions and Research Gaps*

The discussion in the previous sections is about the overview of recent developments in LBM and the widely used hybrid processes associated with laser LBM. Researchers have contributed in many directions of pure LBM and hybrid-LBM. The importance of micro-channels in various fields is also reviewed along with several fabrication techniques used to fabricate micro-channels in different

materials. The following recommendations could be assumed as the future research areas in LBM and its hybrid tree especially fluidic LBM. Most of these conclusions and research gaps can also be seen in [283].

- Hypothetically, the ablation mechanism of LBM is well addressed by many researchers showing that large number of factors contribute to ablation such as laser features, laser parameters, material's properties (thermal, chemical, mechanical), absorptivity, reflectivity, assist gas and much more. Effects of laser parameters and assist gas are deeply investigated but, the researchers have excluded many important material based factors such as absorptivity, reflectivity, latent heats and thermal conductivity of work material which otherwise would surely affect the performance characteristics differently. The consideration of material based properties and the interaction effects on machining characteristics could be a bright research area.
- Physics based phenomenon (absorption, reflection, thermal reaction, chemical dissolution and many more) get involved when laser radiations strike and interact with work material. The explanations of such phenomenon is although quoted by some authors but in randomized order. The identification of such phenomenon is need to address in more categorical viewpoint. The evaluation and validation in scientific manner is additionally more tedious and requires further research to understand the actual mechanisms involved in laser ablation.
- Similarly, type of laser (nanosecond, picosecond and femtosecond) involves varying physics based facts. For example, much complicated physics involved in picosecond laser ablation as compared to other types. Therefore, more detailed experimental and theoretical work is still needed to further clarify the ablation mechanism for each type of laser.
- The logical reasoning of force reduction and high MRR in LAM is well presented but the clarifications of tool life and surface integrity improvements are not properly disclosed. This is due to the non-standardized evaluation procedures adopted especially for tool life. That's why there is conflict among the results. Employing the standard procedures for tool wear may generate even different results than quoted which leads towards a new research direction in LAM.
- HAZ is always there in LBM as well as in LAM. It is, almost all the time, a usual and unwanted characteristic. Temperature distribution and its measurement (in LAM and LBM) is essential to determine HAZ. This measurement is relatively easier during LAM than in LBM. There is much liberty for positioning thermocouple or infrared camera during LAM but LBM offers more restrictions due to confined place. For thin sheets (wafers) the temperature can easily be captured by thermocouple mounted at backside of sheet but does not give the actual heat values. Thus, we need estimations and some assumptions. Furthermore, dealing with thick plates, the use of thermocouple becomes

inefficient. Modern thermal cameras are promising in this regard but offers high resistance for their installations in between the laser head and work station. Therefore, the actual temperature measurements in LBM and their scientific validations might be a future research area. Particularly, measurements of thermal distributions for thick sheets and plates requires more research in future. The temperature measurements ultimately rivet with thermal models. Thus, thermal modeling would become more relied for thick plates.

- During LCM/E there are laser based and chemical etchant based parameters that in combine governs the high precise and good quality ablation. The laser based and etching based parameters closely interconnect with each other. The impact of each set of parameters is researched individually. The optimization of the combined parametric window needs to explore in future research that would serve more effectively to understand the interacting behaviors of laser and etchant. In addition, as the etching mechanism is bit complex in the presence of laser energy, thus, controlling the etching process to obtain structures of desired shape, size, and surface quality is still an issue to be resolved for micromachining applications
- Low MRR and short aspect ratio are still two iconic drawbacks of LCM/E that should be addressed in future research. Although, the etch rate is widely evaluated by many research teams with a fixed ratio of etchant and varying conditions of laser parameters. Experimentation with varying etchant concentrations is very rarely reported. It may yield more improved results especially for high aspect ratio and MRR. The effects of varying chemical concentrations on machined geometries and microstructural modifications is suggested as upcoming research direction.
- Again, the ablation mechanism of UWLA processes involved lot of factors, that's why a mix of inferences are found especially related to ablation rate. The common reason behind this conflict is reported as the particular behavior of the target material. This leads to a wide research gap that could be filled up in future by fine tuning the understanding of ablation phenomenon. This could be achieved by the real time measurements (of temperatures, chemical reactions, phase transformations, plasma pressure, shock wave and many more) and post analysis. One of the possible way to obtain the ablation rate in real time is to measure the acoustic wave at the laser-work-interaction zone by some microphone as experienced by Zhu et al. [209].
- Under the category of UWLA, there is a dense study available to synthesize nano-particles (NPs) of various metals. The process is very commonly attributed to yield NPs of metals with some oxides or carbides due to the presence of water. The future research could be directed to restrict the process for producing pure metal NPs instead of oxides.
- In terms of micro-channels fabrication through laser beam machining (LBM), the produced micro-channels are either undersized or oversized for some geometrical characteristics. It has not been addressed in open literature. The

variation in micro-channel sizes disturbs the fluid flow dynamics and performance during operation. Therefore, the variations in micro-channel geometries caused by LBM can be chosen as a fresh research area.

- The laser beam machining (LBM) produces micro-channels with taperness along channel's sidewalls. Many factors involve in resulting the taperness of sidewalls. However, the taperness is mainly due to Gaussian shape of laser beam. The fabrication of micro-channels with straight sidewalls having 90 degree angle is very difficult to produce through LBM. The future research in this direction may be carried out to produce vertical sidewalls of micro-channels.

Laser Beam Micro-milling of Micro-channels in
Aerospace Alloys

Darwish, S.M.H.; Ahmed, N.; Al-Ahmari, A.M. (Eds.)

2017, XXXII, 342 p. 210 illus., 189 illus. in color.,

Hardcover

ISBN: 978-981-10-3601-9